Design of a Low-Cost Anti-Missile Missile

Evan Gersh Nada Himdi Axel Jazzini Petros Famellos Léo Wattebled

Aerospace Systems Design Laboratory
Georgia Institute of Technology, Atlanta, GA, USA

Design of a Low-Cost Anti-Missile Missile

Prof. Dimitri Mavris
Faculty Advisor

Dr. Adam Cox
Research Advisor

Thomas Devlin
Technical Advisor

Emily Herrmann
Technical Advisor

Evan Gersh
Graduate
AIAA# : 1810538

Nada Himdi
Graduate
AIAA# : 1788884

Axel Jazzini
Graduate
AIAA# : 1811397

Petros Famellos
Graduate
AIAA# : 1809967

Léo Wattebled
Graduate
AIAA# : 1809751

Amelia Hoffs
Undergraduate
AIAA# : 1839020

Eric Kim
Undergraduate
AIAA# : 1402816

Cayden Shaffer
Undergraduate
AIAA# : 1179161

Jason Waki
Undergraduate
AIAA# : 1838993

Affordable Response and Reactive Operations Weapon (ARROW)

Executive Summary

This report presents the final design of a low-cost, short-range, ground-to-air missile interceptor called ARROW (Affordable Response and Reactive Operations Weapon). Designed as a defensive response to modern missile threats, the system emphasizes affordability, scalability, and rapid production. The missile achieves a target speed of Mach 3.5 and is optimized for intercepting cruise missiles and short-to-medium range targets within a defined engagement envelope. From the outset, cost was treated not as a post-design filter, but as a primary driver of the design process. A custom parametric cost modeling tool called MCDAT (Missile Cost Data-driven Analysis Tool) was developed to evaluate trade-offs and guide decisions across disciplines from propulsion to payload and avionics. This tool enabled the team to discard infeasible concepts early and converge on a viable solution that meets lethality and performance thresholds without exceeding budget constraints. To further reduce per-engagement cost, salvo modeling was introduced to assess performance in multi-missile scenarios. This approach allowed for a design that favors probabilistic kill optimization over maximizing single-shot capability, resulting in a more economically scalable system for high-density defense. The final concept delivers a defense solution that is affordable, modular, and tailored for wide deployment by military ground forces. This cost-effective missile system was built from first principles and validated through analytical modeling and simulation. The scripts for the Simulation and Modeling Environment used in this project are available : https://github.gatech.edu/lwattebled3/Missile-Competition-2024-2025

Contents

Nomenclature

Abbreviations

α	Angle of attack (deg)
$\dot{\lambda}$	Line–of–sight angular rate (deg/s)
λ	Line–of–sight angle to target (deg)
a_{lat}	Lateral acceleration command (ft/s^2)
a_{long}	Longitudinal (axial) acceleration (ft/s^2)
C_0	Baseline cost coefficient (USD)
C_A	Axial force coefficient
C_D	Drag coefficient
C_L	Lift coefficient
C_N	Normal force coefficient
C_P	Center of pressure location from nose tip (ft)
C_x	Cost of the x-th production unit (USD)
C_{M_l}	Rolling moment coefficient about longitudinal axis
I	Moment of inertia (slug·ft^2)
L	Learning-curve factor (unitless)
m	Mass (lbm)
N	Navigation constant (unitless)
T	Thrust (lbf)
t	Time (s)
t_{SDD}	System Development & Demonstration duration (yr)
V	Velocity magnitude (ft/s)
V_x, V_y	Velocity components in inertial frame (ft/s)
v_{cl}	Closing velocity between missile and target (ft/s)
x, y	Missile or threat position in inertial frame (ft)
MCDAT	Missile Cost Data-Driven Analysis Tool

Chapter 1

Introduction & Motivation

Short and medium-range anti-missile missiles, or interceptors, are a critical component of modern air defense systems, designed to neutralize incoming missile threats before they reach their designated targets. Current systems, such as the Patriot Missile or Israel's Iron Dome, have proven highly effective at intercepting threats. However, the cost of these countermeasures can be unsustainable as the size and frequency of missile salvos grow. [1], [2]

The 2024–2025 AIAA Missile Systems Technical Committee Challenge calls for a new class of interceptors: low-cost, short- to medium-range missiles that maintain credible performance while dramatically reducing unit cost. The challenge is to design a scalable and affordable missile system that can be integrated into current ground-based and naval, mobile and immobile defense networks without compromising coverage or response capability. The goal is to fill the operational gap between expensive, high-end interceptors and the rising volume of threats, providing a sustainable, deployable solution for modern battlefield conditions.

1.1 Project Introduction and Background

Modern aerial combat is increasingly dominated by the use of unmanned systems capable of long-range operations, high speed, and advanced maneuverability. Achieving such performance demands cutting-edge technologies, which in turn drive up the cost of these systems. As a result, interceptors designed to counter these evolving threats have also become more sophisticated and expensive. At the same time, the number of engagements and

the volume of threats launched per attack continue to rise [3]. These trends have transformed modern aerial warfare into a financially intensive conflict, where each engagement is as budget-intensive as physical, leading to a war of attrition. In response, a new operational requirement is emerging: the development of low-cost interceptors. These systems must be inexpensive to manufacture and operate, while still being effective in neutralizing threats. When integrated with multi-launch platforms and advanced tracking systems, such interceptors can shift the economic balance, imposing significant financial strain on adversaries.

This project aims to design a new missile interceptor that delivers high performance at a low cost, capable of countering salvos of threats with loosely defined characteristics. These defining threat parameters result in a broad and diverse design space that must be thoroughly explored to optimize the system's performance and cost-effectiveness. At this early stage, the foundational aspects of the interceptor must be established, as limited information is currently available. Consequently, the design effort follows a conceptual path in which many major decisions will be made. These early choices will significantly influence the interceptor's cost, architecture, compatibility, and overall performance, while also constraining future design parameters within specific bounds. As such, detailed selection and evaluation of particular design parameters will be deferred to the subsequent preliminary and detailed design phases.

1.2 Challenges and Tailored Approach

The United States and its allies face an increasing need for cost-effective, short-to-medium-range missile defense systems capable of countering large salvos of missiles. Current interceptors, such as the Tamir missile, used in the Iron Dome, cost approximately 50,000 dollars per missile [4]. As missile salvos grow in size to overwhelm current missile defense systems, the economic feasibility of using high-cost interceptors becomes a challenge. The development of a more affordable solution has become a necessity. The objective of this project is to design a low-cost interceptor that meets technical and performance requirements while significantly reducing production costs. This effort will focus on delivering a complete system design and engineering analysis for a drop-in low-cost interceptor, compatible with existing land and sea missile launch platforms. This includes the development of a conceptual system design, detailing the physical characteristics and performance metrics to

best meet the mission requirements. The interceptor's key components and disciplines will include propulsion, aerodynamics, trajectory and controls, structures and mass properties, and cost analysis. The deliverables for this project will be a detailed description of the design process, physical and performance characteristics of the final system design and its components, an operational concept, cost estimate, development plan, and necessary support equipment and other resources necessary to comply with the technical requirements [5].

As for the challenges, low-cost missiles mainly have fixed wings without longitudinal and lateral control characteristics and are propelled by solid rocket motors. Their structural components are also based on common and cheap materials that are not renowned for their thermal and structural characteristics. In our case, the interceptor must have adequate maneuvering characteristics that are normally achieved by expensive thrust vectoring control systems or high-sensitivity control surface systems. The aforementioned systems involve throttling of liquid or hybrid engines, and also very expensive active control systems that exceed the budget of our desired missile.

As one can imagine, the team faces a nearly impossible task if conventional design methods are used. Therefore, the chosen approach has been specifically tailored to meet the competition's requirements through two key innovative strategies. First, a cost analysis tool is integrated directly into the design loop alongside the performance-based subsystems. This means that the overall desirability function is simultaneously driven by both performance and cost metrics. Furthermore, uncertainty is introduced into the cost model to reflect the lack of publicly available data on the pricing of specific components, materials, testing procedures, and manufacturing processes. The second, and more critical, enhancement lies in the design space exploration methodology. This process is divided into three stages:

1. Design Space Exploration: In this stage, low-fidelity tools are used to explore a broad range of design variable combinations. The goal is to identify promising regions within the design space and reduce the number of unconstrained or less influential variables.

2. Optimization: The selected baseline design from the first stage is further refined using more accurate, higher-fidelity tools to optimize its performance and cost.

3. Validation: Finally, the optimized design is validated through high-fidelity methods to ensure it meets the original performance objectives.

1.3 Existing Platforms

As specified by the RFP, the interceptor must be compatible with multiple launch platforms and support systems. Additionally, these systems must be both naval-based and land-based, both mobile and immobile. The team created a database of similar systems to compare against each other in order to pick two, one naval-based and one land-based, which can accommodate the missile and provide adequate supporting functions. These systems are as follows:

1.3.1 11-cell Rolling Airframe Missile (RAM) launcher with RBS 70 NG laser guidance

The aforementioned launch system combines the housing and firing mechanism of the 11-cell Rolling Airframe Missile launcher with the sensors of the High Energy Laser, as well as with the laser guidance system of the RBS 70 NG system. The RAM launcher is designed to house RIM-116 Rolling Airframe Missiles 1.1, which are compact and set the upper sizing boundaries for our system, measuring approximately 2.79 meters (9.15 feet) in length, 127 mm (5 inches) in diameter, and weighing around 73.5 kg (162 lbs) each. The launcher is capable of 360° azimuth rotation and an elevation range from –25° to +70°, allowing it to engage threats across a wide range of trajectories. It is typically mounted above-deck on surface ships, often on the hangar roof or upper deck, and is manually reloaded while the ship is in port. Maintenance is designed to be minimal during deployment, with reloading and other maintenance activities typically conducted when the ship is in port. Additionally, the system is designed to operate under a hostile aquatic environment which makes it ideal for naval operations [6].

Figure 1.1: 11 cell RAM launcher

The tracking system the team selected to accompany this launch platform is the RBS 70 NG 1.2. The RBS 70 NG is a versatile laser-guided missile system that have been successfully adapted for naval applications by Saab. Originally developed for land-based air defense, this naval version is deployed on smaller naval platforms such as patrol boats and coastal defense vessels, providing effective short-range protection against threats like UAVs, helicopters, and incoming missiles. These systems utilize laser beam riding guidance, where the missile stays centered within a laser beam projected by the operator, ensuring precision and resistance to electronic countermeasures (ECM). The RBS 70 NG boasts enhancements such as automatic target tracking and improved night and all-weather capabilities, making it highly effective in cluttered and complex maritime environments [7].

Figure 1.2: RBS 70 NG Systems

1.3.2 Iron Dome System

The selected ground-based system is the Iron Dome, with its principal navigation and launch sub-systems 1.3. The Missile Firing Unit (MFU), which is responsible for launching the interceptor missiles used by the Iron Dome defense system, is designed to intercept and destroy short-range threats such as rockets, artillery shells, and mortars. These interceptors are approximately 3.4 meters (11.15 feet) long, with a diameter of 160 mm (6.3 inches), and each weighs around 90 kilograms (198 pounds). The Iron Dome system itself is capable of providing coverage based on 2 radar modes: rotating mode with a full 360° azimuth coverage and sector mode with 120° azimuth coverage. Finally, the range used by the Iron Dome, the EL/M-2084 Multi-Mission Radar (MMR), has a detection range capable of detecting and tracking targets at a range of up to 43.5 miles [8]. This radar is only the prelaunch radar in our case, as the post launch radar has to be laser-guided. The one selected is the previously mentioned RBS 70 NG once more.

Figure 1.3: The Iron Dome Launcher

1.4 Existing solutions

1.4.1 Tamir missile

The best-known example of a missile is the Iron Dome's Tamir missile deployed by the Israeli army [4]. The Iron Dome is operational day and night, whatever the weather conditions, and is capable of withstanding simultaneous and numerous attacks. The Tamir interceptor missile is the central projectile of the defense system. It is designed by Rafael Advanced Defense Systems to intercept short-range rockets, shells, mortars, and drones. The Tamir measures around 9.84 ft, weighs 198.41 lbm, and has a range of 2 to 43 miles. Equipped with active radar and in-flight correction systems, it is capable of targeting and intercepting multiple threats simultaneously. Its maximum altitude is 33,000 feet, and it can be launched from mobile, fixed, or ship-mounted systems. When a threat is detected,

the Tamir destroys the enemy projectile in flight with an explosive fragmentation charge. The Tamir has proved highly effective, with an interception rate of around 90%, protecting infrastructures and populations against short-range attacks. Its production cost is estimated at between $50,000 and $90,000.

Figure 1.4: Tamir missile

1.4.2 VT-1 missile

The VT-1 missile, developed by the Thales group, is another relatively low-cost interceptor missile. It is a key component of the Crotale NG short-range air defense system used by the French armed forces. This missile is designed to intercept aerial targets such as cruise missiles, as well as low-altitude drones. It is a short-range supersonic missile, reaching speeds of up to Mach 3.5. It has a range of up to 7 miles and can engage targets flying at altitudes of 30,000 feet. It features radar and infrared guidance, giving it a high degree of accuracy, with very rapid interception capability and a reaction time of less than 10 seconds. The missile is equipped with an explosive fragmentation charge and a proximity device to destroy targets without the need for direct impact. The VT-1 missile is used in mobile and fixed defense systems and can be implemented on ships. It can be used to protect critical infrastructure, both military and civilian, against short-range air attacks. The system is renowned for its reliability, which is why it has been deployed in armies around the world (South Africa, Saudi Arabia, South Korea, Egypt, and Finland). The production cost of a VT-1 missile is estimated at $340,000.

Figure 1.5: VT-1 missile

1.4.3 AGR-20 missile

The AGR-20 missile, also known as the Advanced Precision Kill Weapon System (APKWS II), is a solid rocket, laser-guided precision strike missile. The missile is optimized for both moving and stationary vehicles, and specializes in being low-cost and causing minimal collateral damage. In order to ensure low cost, the missile is subsonic. It has been adapted for fixed-wing use and can be integrated with the vast majority of USAF platforms. These include both the A-10 Warthog and the F-16, among others. This compensates for its relatively limited range, with a maximum of about 6.8 miles. The APKWS II has a diameter of 2.75 inches and a length of 6.25 feet, making it fairly small compared to other missiles. It is currently capable of using three types of warheads: high explosive, white phosphorus, and illumination. These make this an ideal missile for close-engagement combat situations, such as eliminating drones above friendly forces, and providing support to infantry and artillery. This missile has been in use since October 2012, and its first flight was in May 2013. The APKWS continues to be an important part of the USAF weapons arsenal to this day.

Figure 1.6: AGR-20 Advanced Precision Kill Weapons System

Chapter 2

Requirements

2.1 Request For Proposal Requirements

The overall requirement of this Design Competition is to develop a low-cost anti-missile missile. Emphasis should be on minimizing system cost while meeting system performance and effectiveness requirements.

The technical requirements that were provided by the customer RFP can be divided in different categories. Some of them concern the performance of the interceptor itself, some of them are about the characteristics of the threats that should be intercepted, and others concern production, logistics, and operation.

In terms of the interceptor requirements, some of the expected performance of the vehicle is described in the request for proposal. For instance, the missile installation shall have a horizontal defense radius of 5 miles and provide 360° azimuthal coverage. Moreover, the interceptor shall have a maximum engagement altitude of 30,000 feet, and the selected design shall offer the capability to incorporate command data links and receive in-flight updates.

In terms of the threat requirements, the enemy missile can be assumed to have the following characteristics:

- Ground ranges of 0.5 to 60 miles (1 to 100 km)
- Up to 3 g's of non-ballistic maneuvering capability
- Speeds up to Mach 3

- Unitary missile
- Minimum size: 4 inches in diameter, 8 feet in length, 100 lbm mass
- Maximum size: 24 inches in diameter, 20 feet in length, 4000 lbm mass

Finally, regarding the production, logistics, and operation requirements, the missile shall be compatible with safe storage, transportation, and handling requirements for a minimum of 10 years without maintenance. Furthermore, the interceptor cost should not exceed $10k per missile. The RFP defines the production rate as 1000 missiles to be produced each year for 10 years, plus 100 missiles for developmental testing. Other important requirements concern compatibility with existing launch platforms. The interceptor must be capable of being launched from existing fixed, ground-based launcher installations, but also, if possible, from existing mobile ground-based launchers as well as ship-mounted launchers. Finally, the missile must be able to go from a dormant state to launch in less than 1 second.

A summary of the requirements can be found in Table 2.1, below.

Table 2.1: Level 1 requirements collated from the RFP

Category	Rqmt No.	Requirement Description
Performance of the interceptor	L1-001	The missile installation **shall** have a horizontal defense radius of **5 miles**.
	L1-002	The missile installation **shall** provide **360° of azimuthal coverage.**
	L1-003	The missile installation **shall** intercept missiles up to **30,000 feet**.
	L1-004	The interceptor design **shall** have the option to include **command data links** or **in-flight updates**, without mandating their inclusion.
Threat characteristics	L1-005	The missile **shall** intercept a target with ground range **between 0.5 and 60 miles**.
	L1-006	The missile **shall** intercept a target missile non-ballistic maneuvering at **up to 3 g's**.
	L1-007	The missile **shall** intercept a target missile at speeds of **up to Mach 3**.
	L1-008	The missile **shall** intercept a target missile with a minimum size of **4 inches in diameter, 8 feet in length and a 100 lbm mass** and a maximum size of **24 inches in diameter, 20 feet in length and a 4000 lbm mass**.
Production, logistics and operation	L1-009	The missile, including energetics and/or propellants, **shall** be compatible with safe storage, transportation, and handling requirements for a minimum of **10 years without maintenance**.
	L1-010	The missile shall be produced at a rate of **1000 units per year** for a period of **10 years**, in addition to **100 units for developmental testing**.
	L1-011	The cost of the interceptor **shall not exceed $10,000 per missile**.
	L1-012	The anti-missile missile **shall be compatible with existing launch platform**.
	L1-013	The interceptor **must be capable** of being launched from current **fixed, ground-based launcher installations**, but also, if possible, from existing **mobile ground-based launchers** as well as **ship-mounted launchers**.
	L1-014	The missile **must be able** to go from a dormant state to launch **in less than 1 second**.
	L1-015	The system development **shall begin no later than October 2025**, and the system shall achieve Initial Operational Capability (IOC) **no later than December 2030**.

2.2 Derived Requirements

From the requirements defined in the RFP, it is possible to derive additional requirements that are essential to successfully complete the missile design process. As seen in the previous section, some requirements define the characteristics of the threat and create constraints for the interceptor that should be respected. In the same vein, the requirements concerning the compatibility with existing launch platforms further constrain the design of the interceptor.

2.2.1 Launch Platform Derived Requirements

The RFP imposes the compatibility of the interceptor with existing launch platforms (ground-based but also ship-mounted platforms). The two systems that are picked to accommodate the missile and provide adequate supporting functions are the 11-cell Rolling Airframe Missile (RAM) launcher and the Iron Dome system. This compatibility requirement is very stringent and creates new constraints for our design in terms of missile size, threat detection range, time to intercept, or even launch/initial velocity. The missile length is constrained by the RAM Block 2 length and thus cannot exceed 9.45 feet. The missile diameter also needs to match the RAM and Iron Dome canister diameter, and should be less than 5 inches. In terms of mass, the two systems are designed to support missiles weighing between 160 lbs and 200 lbs.

The minimum detection range of incoming threats is also constrained to 5-10 km based on Iron Dome and RAM engagement envelope. The interceptor should also be able to support an initial velocity greater than 131 feet per second to support the typical cold/gas ejection from the canister performed by these launch platforms.

Finally, the final design must withstand shipboard vibration and shock as it will be launched from a ship-mounted platform and will operate in a naval environment.

2.2.2 Threat Derived Requirement

In terms of the derived performance requirements, the propulsion system shall be adequately defined so that the interceptor can protect the entirety of the defense area defined in the RFP (defense radius of 5 miles and maximum engagement altitude of 30,000 feet).

In addition, the aerodynamics and flight control mechanisms of the missile must provide sufficient lift and maneuverability capabilities to intercept the type of threat describe in the RFP. In order, to successfully perform endgame maneuvers, the interceptor shall have

about 3 times the maneuverability of its target [9]. Therefore, as the enemy missile can be maneuvering at up to 3 g's, our interceptor must have 9 g's of maneuverability in the endgame.

Finally, the interceptor velocity should be greater than or equal to the threat missile velocity. As the threat can reach a speed of up to Mach 3, our design must also be able to travel at Mach 3.

2.2.3 Production, Logistics and Operation Derived Requirements

The production, logistics, and operation requirements also create additional requirements for the interceptor. As the selected design should be compatible with safe storage, transportation, and handling requirements for a minimum of 10 years without maintenance, it creates, for instance, constraints on the material used and on the type of propulsion. Corrosion-resistant materials should be selected for external casing and critical components, and solid propulsion should be favored to minimize the risk of leakage and maintenance.

In addition, the cost requirement that is very stringent induce that COTS (Commercial Off-The-Shelf) components should be used wherever it is feasible to decrease the total cost. Exotic materials should also be avoided, and only cost-effective options should be evaluated. Another point is that simplified and innovative manufacturing techniques should be considered as much as possible.

Finally, the missile must be able to go from a dormant state to launch in less than 1 second. Therefore, electronic components of the interceptor must remain in low-power sleep mode, not powered off during standby. The use of pyrotechnic or other rapid-start mechanisms for the propulsion system should also be favored.

2.2.4 Design Challenges

As shown in the previous section, many requirements have to be satisfied to obtain a satisfying design. Some of these requirements are really challenging and are going to reduce a lot the number of feasible alternatives.

The first challenge is the compatibility with existing launch platforms, both ground-based and ship-mounted. As explained in section 2.2.1, it implies new requirements in terms of missile size, threat detection range, and even launch initial velocity.

However, the most challenging requirement is undoubtedly the cost requirement. As

stated in the RFP, the cost of the interceptor shall not exceed $ 10,000. By reviewing a database of more than a hundred different missiles, it is possible to display the number of existing missiles in different cost ranges of cost as shown in Figure 2.1.

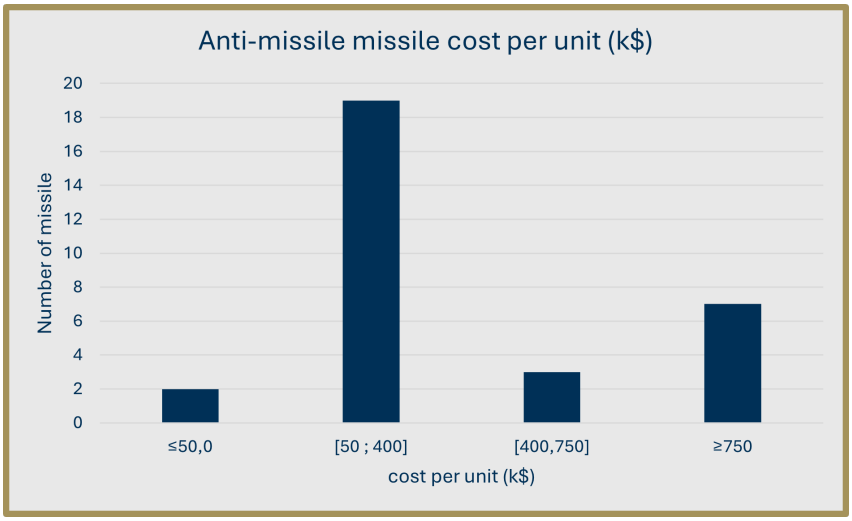

Figure 2.1: Repartition of the number of missiles per range of cost

By exploring the database in more detail, it can be found that only one design satisfies the cost requirement: the Trembita Cruise Missile (figure 2.2). Yet, this interceptor is non-guided and cannot exceed Mach 0.6. Its performance is not acceptable and does not satisfy the other requirements defined in the RFP.

Figure 2.2: Trembita Cruise Missile

The least expensive missile in the database that has performance capabilities very close to what is stated in the RFP is the APKWS missile. However, the cost per unit for this interceptor is $ 22,000. Therefore, no missile in the database satisfies both the cost and the performance requirements. A new methodology should be developed to better assess the

cost of the interceptor during the design process, and innovative solutions to reduce the cost should be evaluated.

Chapter 3

Design Space Exploration

As the system is a combination of multiple subsystems that interact with each other, the design process involves a high number of design variables that are correlated and sometimes enforce constraints on each other. To identify a design space, the subsystems are broken down into the lowest possible level and analyzed independently, with safety factors that account for their effects on the complete system. Additionally, the ranges of the design variables are to be arbitrarily set at the beginning of the design space exploration. These ranges are identified by literature reviews and databases.

3.1 Planned Approach

As mentioned previously, to independently explore the design space and run multiple cases in parallel to maximize the amount of extracted information, the system has been broken down into some primary subsystems that mainly drive performance and cost. The primary subsystems driving performance are not the same as the ones selected for the cost evaluation. To that extent, the independent subsystem analysis yields insights and statistics on trends of the design space, where the team should focus more. This technique allows for a more methodical design process that minimizes the number of cases run in design space areas that might not be of interest.

After gaining some initial information about the subsystem's areas of interest, the team can now focus on filtering the design alternatives on the basis of cost and performance. The performance analysis tool starts with the generation of multiple threat scenarios based on the RFP requirements and the derived requirements, as will be explained in later subsections

of this report. The next step is analysis of all the different threat profiles by a proportional guidance tool that essentially translates all the threat scenarios into acceleration time series for different movements of the interceptor. The previous two steps allow the team to integrate two independent systems, the threat and the interceptor, into one mission envelope which then can generate multiple scenarios and create a system of systems approach to the design process. By the end of this step, the team has created a library of all the acceleration time series per axis for many threat scenarios, with some constraining cases standing out.

The next step of the performance filtering tool is the comparison of this acceleration library to the achievable ones of every single design that was generated. In the end, a matrix of alternatives is created for the design variables of the control surfaces, the forebody aerodynamic design variables, the propulsion design variables, and the structures design variables. The next step is to create multiple design and assess the capabilities of every subsystem independently. This translates to running aerodynamics analysis and creating the aerodynamic decks independently of the interceptors propulsion subsystem design variables, given that some constraints are met. At the end of the analysis, the interceptor can be translated into a set of properties that, when used by a trajectory tool, provide the achievable maximum and minimum acceleration time series. Finally, these two time series are compared against the full library of needed accelerations created by the threat envelope and proportional guidance tool to identify the percentage of threat scenarios an interceptor was able to respond to.

In addition to performance filtering, a cost filtering mechanism is implemented to ensure compliance with budget constraints. To achieve this, a parametric, data-driven cost analysis tool has been developed, as detailed in Section 3.2. This tool enables early-stage cost assessment of each design, facilitating better cost control to meet the $10,000 requirement set by the RFP. Once both performance and cost evaluations are completed, the designs that best satisfy both criteria can be identified, allowing for an optimized selection process that balances effectiveness and affordability.

3.2 Cost

The cost limit defined in the request of proposal is one of the most constraining requirements. In fact, each interceptor should have a cost that does not exceed $ 10,000. This amount takes into account the production cost, the assembly and test cost as well as the operational

cost per launch (including propellant cost, igniter launch, failed launches, battery costs, and so on). Therefore, there is a need for a filtering of the design space based on the cost. Many alternatives will be too expensive and can be put aside early in the design process. To do so, a cost analysis tool should be developed in order to obtain a good estimate of the different costs of an interceptor. The implementation of the cost analysis tool in the first steps of the design process is one of the main differences between the approach presented in this document and the traditional approach to designing a missile. In fact, typically the cost assessment occurs after the selection of the feasible design. In this new methodology, the cost is used as a criterion to proceed to the down-selection and the reduction of the design space (figure 3.1)

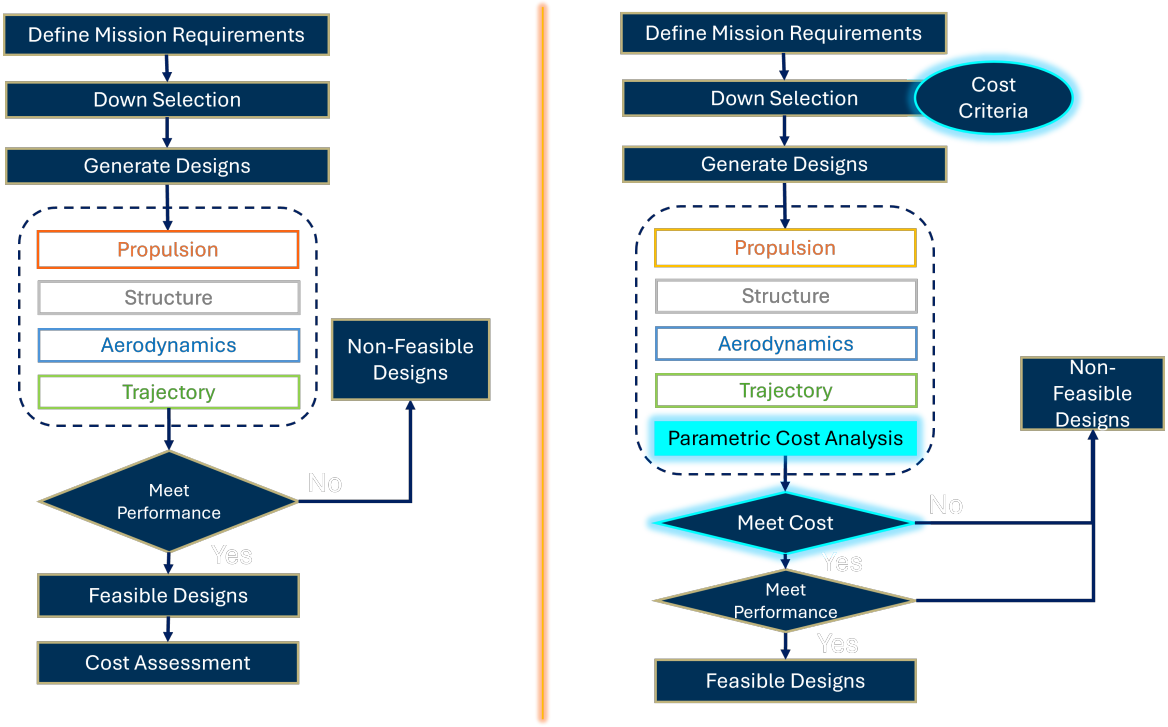

Figure 3.1: Two different approaches for the missile design process

The cost tool developed by the team is named MCDAT (Missile Cost Data-Driven Analysis Tool). It integrates multiple analytical approaches to provide comprehensive cost predictions based on over 25 input parameters. MCDAT is composed of two main parts. The first part has the goal of obtaining an estimate of the first unit production cost and of the mean production cost of the interceptor over a 10-year period. To do so, several methods are implemented (machine learning algorithm, historical breakdown, cost estimators..).

The production cost is then fed into a learning curve model to predict unit cost trends over a 10-year period. All outputs are subjected to uncertainty quantification to account for variability and improve the robustness of the estimates. The second part of the tool uses statistical methods to find the maintenance, tooling, and operational costs. The outputs of the tool include the first unit production cost, the mean cost of a unit over a period of 10 years, a cost breakdown, and uncertainty intervals. The global framework of MCDAT is presented in Figure 3.2.

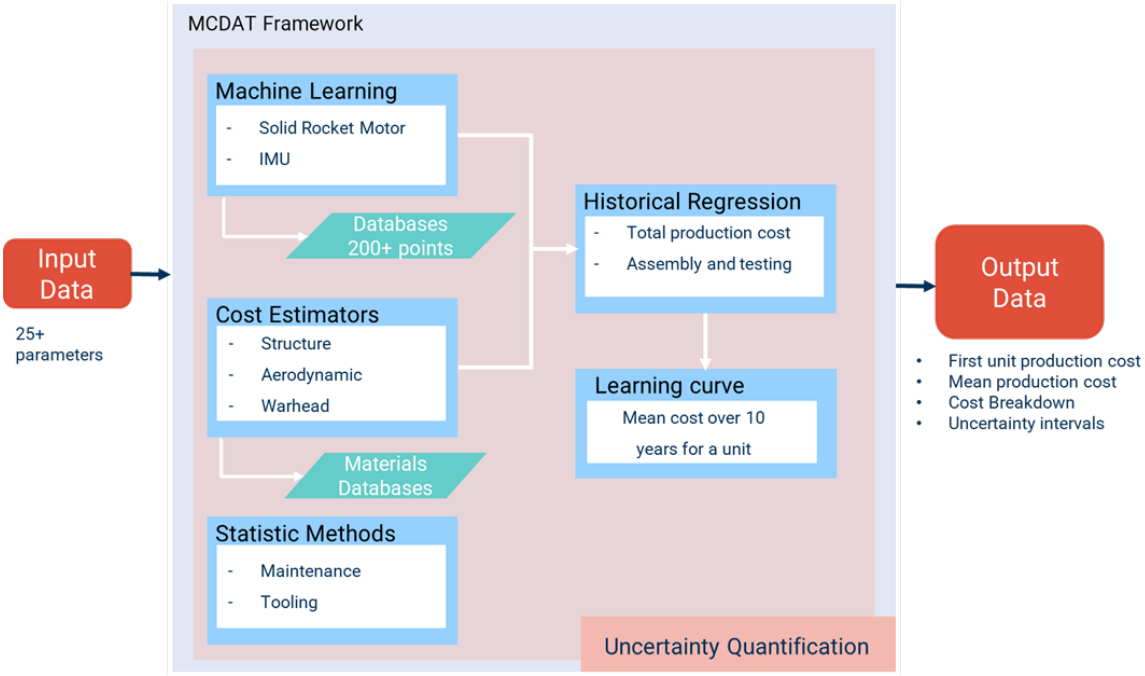

Figure 3.2: MCDAT Framework

3.2.1 First unit production cost

In order to obtain the first unit production cost of an interceptor, the approach used in the tool MCDAT is a bottom-up analysis. The missile is broken down into subsystems, and a parametric cost model is implemented for each subsystem. The different subsystems defined are the following:

- Solid Rocket Motor (SRM)
- Structure
- Seeker

- Avionics (IMU and flight computer)
- Warhead
- Additional components

For each of these parts of the interceptor, a different methodology is implemented to estimate the cost.

For the seekers, the solid rocket motor and the IMU, off-the-shelf components are favored in order to reduce the total cost. Therefore, data of existing systems are used, and the cost of the SRM and the cost of the IMU are obtained using a machine learning algorithm. The Random Forest algorithm is used and trained on a database of more than a hundred points. This specific algorithm is selected for different reasons. It is very efficient for small databases and additionally accounts for non-linear behavior.

The cost of the structure and aerodynamics are estimated based on the volume of material needed as well as the cost of the material. The cost of the warhead is estimated assuming a blast fragmentation warhead.

Once the cost of the previous subsystems is known, the total production cost can be estimated using a historical cost breakdown. 17.5 % of the total cost is driven by the SRM and 6% of the total cost is driven by the structure and aerodynamics, and 7.5% is driven by the warhead. These three parts account for approximately 31 % of the total production cost [10]. For the remaining subsystems, percentages of the total production cost are used to estimate the cost.

Structure

The cost of the structure encompasses several parts of the missile. The first one is the nosecone, and the second one is the fuselage. In order to estimate their cost, the volume of material needed is computed and is then multiplied by the average cost of the material (equation 3.1).

$$Cost_{structure} = V_{structure} Cost_{material} \tag{3.1}$$

A database with the average cost of several materials typically used for missiles was created using data from the last ten years. A snapshot of this database is presented Figure 3.1

Material	Mean (USD/lbm)	Min (USD/lbm)	Max (USD/lbm)
Aluminium	0.97	0.86	1.07
Fiber glass	0.75	0.68	0.78
SiC	0.62	0.58	0.65
B_4C	22.34	21.64	23.04
Steel	0.25	0.23	0.27
Graphite	0.41	0.35	0.47
Plastic	0.71	0.69	0.73
Phenolic composite	2.18	2.12	2.24
Titanium	3.81	2.96	4.65
Carbon composite	31.57	30.71	32.42
Carbon fiber	11.59	11.34	11.83
Tungsten	10.23	9.32	11.13

Table 3.1: Costs of Various Materials in USD/lbm

Aerodynamics

The cost of the aerodynamic subsystem can be broken down into two distinct categories. The first one is the control surfaces, while the second one is the forebody. As the forebody can be modeled by the structures subsystem, by using the same design variables and making the assumption that the cost is the material mass times the price of the material per unit mass times a safety factor to account for additional unmodeled components,such as fasteners and other minor elements.

The cost of the control surface is modeled similarly, with the additional cost of control mechanisms (servos, gearing, and hubs). This cost is based on the interpolated data extracted from online libraries and is based on the maximum hinge moment acted upon each fin. An additional safety factor is used to account for gearing and hub costs.

Propulsion

The cost of the propulsion subsystem is primarily driven by the solid rocket motor (SRM). To develop an accurate and efficient cost estimation model for the SRM, a comprehensive database was first compiled, containing detailed characteristics and costs of over 100 SRMs derived from manufacturers' data [11]. A preliminary sensitivity analysis was then performed using Pearson's correlation method, identifying the primary linear relationships between SRM characteristics and their costs. To capture more complex, nonlinear dependencies and to enhance prediction accuracy, a series of machine learning algorithms were evaluated, ultimately identifying Random Forest as the most effective surrogate model. Random Forest was selected for its ability to model nonlinear relationships robustly, perform

effectively on relatively small datasets, and exhibit resilience against overfitting, achieving a high predictive performance with an R^2 value of 0.96. The final key variables influencing SRM cost are summarized in Table 3.2.

Table 3.2: Variables driving the SRM Cost

Variables
Total Impulse
Motor Diameter
Motor Length
Maximum Thrust
Average Thrust
Motor Mass
Propellant Mass
Volume
Mean Impulse
Maximum Impulse

However, the variables presented in Table 3.2 are not directly derived from the Design of Experiments (DoE). Instead, they are obtained through the propulsion analysis detailed in Section 3.3.4. This ensures that the cost-driving parameters used in the model accurately reflect the physical and performance characteristics of the propulsion subsystem.

Avionics

The cost of the avionics subsystem is significantly influenced by the Inertial Measurement Unit (IMU). To effectively estimate IMU cost, an extensive database of over 100 IMUs was compiled, incorporating technical specifications and pricing data from various manufacturers. Initially, a sensitivity analysis using Pearson's correlation was conducted to identify primary linear relationships between IMU characteristics and associated costs. Due to the complexity and highly nonlinear relationships within the IMU dataset, several features, such as temperature range, were discarded because they introduced noise without significantly improving prediction accuracy. Furthermore, new composite metrics were generated from existing parameters to better capture essential characteristics and enhance model representativeness. Subsequently, multiple machine learning techniques were evaluated, and the Random Forest algorithm was determined to be the most effective surrogate model. The final parameters influencing IMU cost are summarized in Table 3.3. The total cost of the avionics subsystem was then computed as the sum of the predicted IMU cost and the estimated cost of the flight computer, the latter assumed to represent 17.5% of the overall missile cost based on historical data [10].

Table 3.3: Variables driving the IMU Cost

Variables
Angular Bias Instability
Acceleration Bias Instability
Angular Bandwidth
Acceleration Bandwidth
Angular-Acceleration bandwidth Ratio

Warhead

To estimate the cost of the warhead, a blast fragmentation-type warhead is assumed. The total cost is mainly driven by the mass of the metal casing and the mass of the explosive. The cost of the fuze should also be added, as it is necessary to detonate the explosive. In order to maximize the kinetic energy and thus the fragment velocity, the charge-to-metal ratio should be set at 1 [2]. Therefore, the explosive mass and the metal casing are assumed to be equal (equation 3.2)

$$m_{casing} = m_{explosive} = \frac{m_{warhead}}{2} \tag{3.2}$$

Once the mass of the casing and the mass of the charge are known, the cost can be estimated using a similar approach as the structure and the aerodynamics.

$$Cost_{warhead} = m_{casing} Cost_{material} + m_{explosive} Cost_{explosive} \tag{3.3}$$

The cost of the fuze is assumed to be equal to the cost of the warhead. This assumption comes from a cost breakdown in Fleeman's book in which the fuze and the warhead represent the same percentage of the total cost of the missile [10].

Finally, the total cost for this subsystem is obtained by summing the cost of the warhead and the cost of the fuze.

Total first unit production cost & Assembly and test cost

Once the cost for the solid rocket motor, the structure, the aerodynamics, and the warhead is computed, it is possible to obtain an estimate of the first unit production cost of the interceptor using a historical breakdown. Typically, the SRM corresponds to approximately 17.5% of this cost, the structure and aerodynamics correspond to approximately 6% of the first unit production cost, and warhead accounts for 7.5%. Therefore, the previous

subsystems together account for 31 % of the first unit production cost.

Moreover, as stated in Fleeman's Missile Design book [10], the system assembly and test cost represents approximately 10 % of the production cost. This percentage is used to obtain an estimate.

Other subsystems

The cost of the other subsystems is not going to be modeled directly and is computed using percentages of the first unit production cost. Among these additional subsystems, we can find the seekers, the thermal protection, the batteries, and the flight control computer. The relative importance of each of these subsystems in the final cost breakdown is listed below:

- Seekers account for 27.5% of the first unit production cost
- Thermal protection accounts for 2.5% of the first unit production cost
- Batteries account for 2.5% of the first unit production cost
- Flight control computer accounts for 17.5% of the first unit production cost

Dummy variables will be used to simulate their effect on the trajectory of the missile. Both of these subsystems will be represented as volume masses placed inside the rocket. Their effects will be simulated through the mass properties tool by influencing the mass properties and enforcing some additional space constraints.

3.2.2 Learning curve and Long Term Cost

The next step is to incorporate the learning curve in order to obtain a more accurate estimate of the missile production cost. The learning curve reflects the efficiency gains achieved as production scales. As more units are produced, workers and processes become more proficient, leading to reductions in time, labor, and material waste, which ultimately lowers the overall cost per unit. By accounting for these improvements, we can make more accurate projections, optimize resource allocation, and better plan for long-term production. This is especially important in the case of this interceptor. The RFP states that 1000 missiles should be created each year for ten years. Initial production runs may be costly, but improve significantly over time. The equation for the learning is linking the cost of unit x, the cost of the first unit, and a learning factor L as shown in equation 3.4.

$$C_x = C_{1st} L^{\log_2(x)} \tag{3.4}$$

With C_x the cost of unit x, C_{1st} the cost of the first unit, and L the learning factor.

Typically, there is a labor-intensive learning curve if L is under 0.8 and a machine-intensive learning curve if L is above 0.8. In this study, L is fixed equal to 0.8 to balance the two. Contributors to the learning curve include:

- Labor force motivation and efficiency
- Tooling, manufacturing process, and production rate
- Components maturity and complexity

3.2.3 Uncertainty quantification

In order to improve the robustness of the estimates and give a range of costs, especially for the selected final design, uncertainty quantification is performed by the tool, MCDAT. The potential variation of the cost is taken into account while computing the SRM and the IMU cost, as well as the cost of the structural and aerodynamic subsystems. For the other subsystems, the lake of data (for the warhead, for instance) or the methodology used to estimate the cost (historical breakdown for seeker and additional components) have prevented us from developing a reliable uncertainty quantification model.

SRM and IMU Uncertainty Quantification

To rigorously quantify the uncertainty in the cost estimation models for both the solid rocket motor (SRM) and the inertial measurement unit (IMU), a bootstrapping-based approach was implemented. For each subsystem, 100 surrogate models were trained by resampling the original dataset with replacement, generating new training subsets of equal size. This technique preserved the statistical properties of the original data while introducing controlled variability, enabling the assessment of how fluctuations in input data affect model predictions. Each of the 100 Random Forest models was then used to predict costs for a fixed set of input configurations. The resulting ensemble of predictions formed a distribution for each case, from which key statistical indicators—including the mean, standard deviation, and 95% confidence intervals—were derived. This analysis captured the epistemic uncertainty driven by limited data and model variability. The 95% confidence interval provided a

robust measure of prediction reliability, offering valuable information about the range within which the true cost is expected to lie. Ultimately, this uncertainty quantification process significantly enhanced the interpretability and credibility of the cost models for both the SRM and IMU subsystems. The associated uncertainty intervals for the sample of SRM cost predictions are illustrated in Figure 3.3. The horizontal lines, respectively, represent the 75, 50, and 25 quartiles.

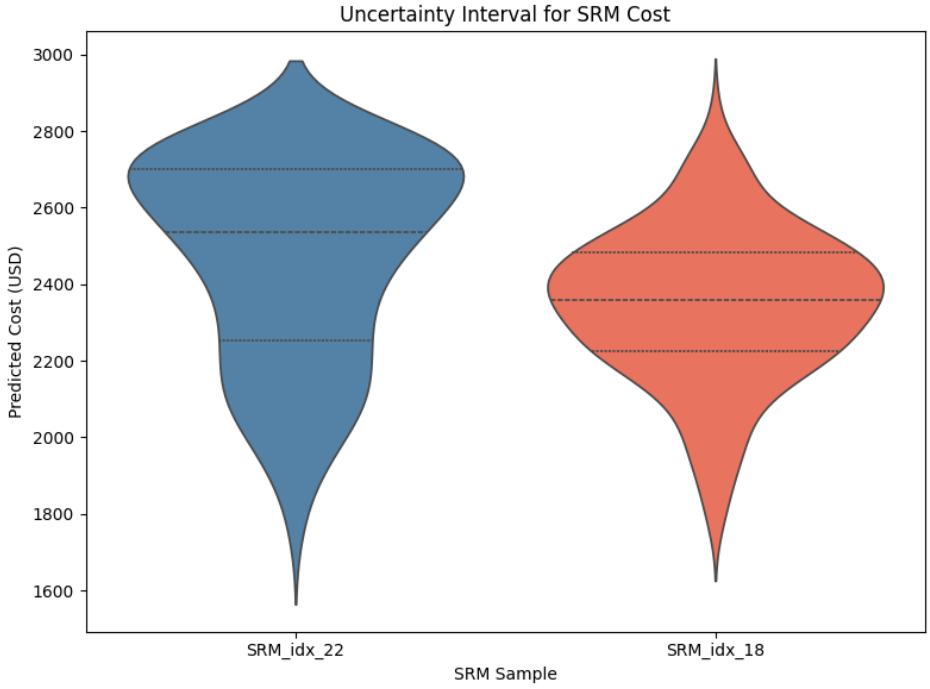

Figure 3.3: Uncertainty Quantification for SRM Cost

Aerodynamic and structure uncertainty quantification

To quantify the uncertainty regarding the aerodynamic and structural subsystems, the variation of the material price over the years is taken into account. For each material in the database created, a minimum, a maximum, and a mean value are determined by looking at the variation of the material cost (in USD/lbm) over the past 20 years.

In order to obtain the most optimistic value, only the minimum cost of the material is used. In the same way, the most aggressive value is found by using the maximum cost of the material. Therefore, the cost interval for each of these subsystems can be determined.

To obtain the repartition of the cost of the aerodynamic and structural subsystems, a probability distribution is used. Since only a minimum, a maximum, and a mean value are

available, but not a standard deviation or full dataset, we are dealing with limited statistical information. The most appropriate probability distributions in this case are the ones that can be defined by just min, max, and mean. Therefore, a PERT distribution (modified Beta distribution) was selected. This distribution is skewed and flexible. It favors values near the mean rather than equally weighting all values, and is well-adapted to this cost analysis.

3.2.4 Life Cycle Cost Estimation Methodology

In this subsection, the methodology employed in the tool MCDAT to estimate the principal components of the missile's life cycle cost (LCC), including Research, Development, Testing, and Evaluation (RDT&E), maintenance, tooling, and operating costs, is presented. Each of these costs is computed based on statistical modeling, historical cost data, and missile system characteristics.

Research, Development, Testing, and Evaluation (RDT&E)

First of all, the RDT&E cost accounts for the initial development of the missile, including design, prototyping, testing, and qualification. This cost is modeled using a power-law cost estimation formula:

$$\text{RDT\&E Cost} = C_0 \cdot t_{\text{SDD}}^{1.9} \tag{3.5}$$

where:

- C_0 is a baseline cost coefficient, set to \$20 million,
- t_{SDD} is the duration of the System Development and Demonstration phase (in years),
- The exponent 1.9 captures non-linear growth in cost with program duration.

This formula reflects and captures increasing engineering effort and complexity over longer development timelines.

Maintenance Cost Estimation

Maintenance costs can be divided into two parts. They include both preventive and corrective actions over a projected service life of 30 years.

Preventive Maintenance

Preventive maintenance includes daily, weekly, and monthly checks to detect directly visible information of troubles. During this type of maintenance, inspection for damage, wear, dirt, and missing parts, cleaning, and a check of fuel leaks through a sniff test are performed. Fin response of the missile is also tested. The cost associated with preventive maintenance is mainly the personnel cost. Using the example of the NIKE AJAX missile [12], it was determined that an average of 12 technicians are responsible for a battery (which is assumed to be equivalent to 54 missiles based on the Iron Dome data). The details of the required personnel is as follow: an average of 1 Missile Warrant Officer per battery, an average of 2.5 Electrical Maintenance Chief per battery, an average of 2.2 Mechanical Maintenance Chief per battery, an average of 2 Generator Operator per battery, an average of 3.3 Engineering Equipment Specialist per battery and an average of 1 Air Compressor Operator per battery.

The cost of the preventive maintenance is computed as:

$$\text{Preventive Cost per Missile} = \text{Salary} \times \text{Tax Multiplier} \times \text{ Number of Years} \times \left(\frac{\text{Crew Size}}{\text{Missile Battery Size}} \right) \tag{3.6}$$

where:

- Salary is the average annual technician salary ($52,000),
- Tax Multiplier accounts for employer costs (e.g., benefits) and is set to 1.4,
- The crew is responsible for the upkeep of an entire battery (e.g., 12 technicians for 54 missiles).

Corrective Maintenance

Corrective maintenance is another type of maintenance that happens every 10 years. It corresponds to in-depth maintenance and replacement of defective subsystems. The costs associated with this type of maintenance are the personnel cost and the subsystem replacement cost. The subsystem's replacement cost is estimated using a Monte Carlo simulation across the 30-year life cycle, divided into three 10-year periods. The following parameters are considered:

- Probability of failure per 4-month period and subsystem (e.g., seeker, IMU, motor),
- Cost of replacing each subsystem,

- Likelihood of multiple component failures per event, sampled using a truncated normal distribution.

Seeker, IMU, fuze, and to a lesser extent, datalink, control surfaces, and motor are considered to be the subsystems that are the most likely to be damaged and to be replaced. Therefore, a probability of replacement of 0.2 is set for the first three, and a probability of 0.15 is set for the last three.

Each simulation run computes the expected cost of unplanned maintenance events and adds an extra end-of-decade replacement cycle for realism. The final cost is obtained by averaging the results across 1,000 Monte Carlo iterations.

Operating Cost

Operating costs include logistics, storage, handling, personnel training, and other recurring support expenses not captured by maintenance. Following cost estimation practices, the operating cost is modeled as a fixed proportion (10%) of the total life cycle cost, excluding the operating cost itself. The formula is:

$$\text{Total LCC (estimated)} = \frac{\text{Acquisition Cost} + \text{RDT\&E Cost}}{0.9}, \tag{3.7}$$

$$\text{Operating Cost} = 0.1 \cdot \text{Total LCC (estimated)} \tag{3.8}$$

This proportion reflects historical data on missile programs, where support costs typically represent 10% of the life cycle cost [13].

Overhead Costs

Overhead costs are added as a markup to O&S to account for administrative, management, and indirect operational expenses. These are estimated as:

$$\text{Overhead Cost} = 0.13 \cdot \text{Operating Cost} \tag{3.9}$$

This percentage is consistent with cost models used in defense procurement agencies.

3.3 Performance

3.3.1 Trajectory Integrator

To assess the performance of the generated designs, a trajectory simulation framework is required. In the first phase of design space exploration, all trajectory simulations are constrained to two dimensions with two degrees of freedom. The primary objective of this phase is to derive performance requirements for the missile interceptor based on the specified threat parameters. To achieve this, a threat scenario envelope has been generated, providing a comprehensive representation of potential adversary trajectories. Additionally, a proportional navigation algorithm has been implemented to evaluate interceptor guidance and engagement performance against these threats.

Threat Scenarios Generation

To evaluate the performance of the proposed designs, it is essential to generate a diverse set of threat scenarios. The Request for Proposal (RFP) specifies key threat performance requirements, including a maximum Mach number of 3 and defined launch positions. The overall approach is outlined in the Figure 3.4

In the initial phase of design space exploration, trajectory simulations are conducted within a two-dimensional framework. A Python script was developed to compute physics-based trajectories for potential threat scenarios, with each threat characterized by key parameters outlined in Table 3.4. To systematically explore the threat space, a Design of Experiments (DoE) approach was implemented, generating 8,000 threat configurations using Latin Hypercubes.

The DoE incorporated key thrust curve characteristics—including maximum thrust, rise time, plateau duration, and decay rate—under the assumption of a solid rocket motor. While this assumption represents a limitation, it remains sufficient to capture both feasible and extreme threat scenarios, ensuring a comprehensive assessment of potential threats within the defined parameter space.

The Python script identified threats that impact the designated defense area while adhering to the RFP constraints. To further enhance computational efficiency, a surrogate model predicting the impact location was developed using the Random Forest algorithm. This model enabled a large-scale Monte Carlo simulation of 100,000 threat scenarios. From these, 7,311 scenarios satisfied all RFP requirements and will be utilized in the subsequent

performance analysis phase.

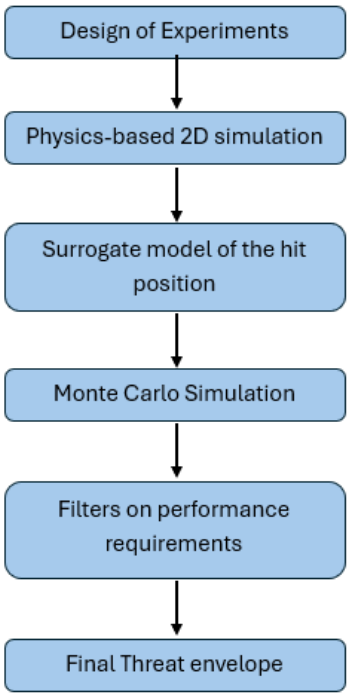

Figure 3.4: Threat Envelope Design Process

Table 3.4: Threat Scenarios - Design of Experiments Variables

Parameter	**Range**
Weight (lbm)	220 - 8818
Cross Area (in^2)	12.6 - 452
Drag Coefficient	0.3 - 0.7
Max Thrust (lbf)	224 - 5620
Rise Time (s)	0.5 - 2
Plateau Duration (s)	2 - 10
Decay Rate	100 - 5000
Initial Velocity X (ft/s)	0 - 4921
Initial Velocity Y (ft/s)	0 - 1640

3.3.2 Missile Engagement Phases and Guidance Framework

The missile flight is divided into three main phases: the **launch phase**, the **boost phase**, and the **guidance phase** where Augmented Proportional Navigation (APN) is applied.

Launch Phase – This phase spans the first 0.5 seconds of flight, during which the missile detaches from the launcher and achieves a minimum safe velocity to ensure clear separation from the launch platform.

Boost Phase – The boost phase corresponds to the duration of the solid rocket motor burn. Its primary purpose is to provide the missile with sufficient thrust to climb, accelerate, and gain altitude before transitioning to the guidance-controlled segment of flight.

Guidance Phase – Following boost, the missile enters the tracking or guidance phase governed by Augmented Proportional Navigation (APN). Proportional Navigation (PN) is a widely used guidance law that commands an acceleration perpendicular to the line-of-sight (LOS) to the target, proportional to the LOS rate. Mathematically, the PN law is expressed as:

$$a_c(t) = N v_c \dot{\lambda}(t) \tag{3.10}$$

where $a_c(t)$ is the lateral acceleration command, N is the navigation constant, v_c is the closing velocity, and $\dot{\lambda}(t)$ is the LOS angular rate.

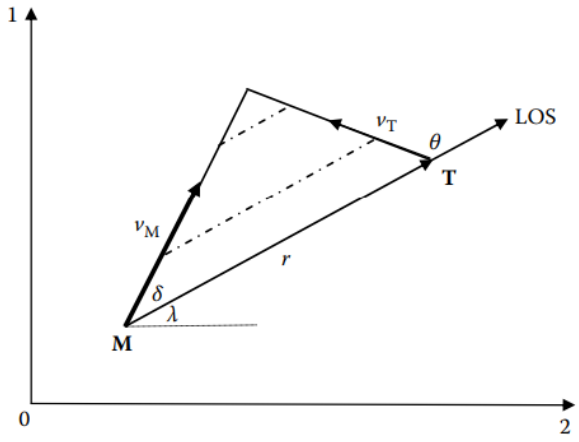

Figure 3.5: Engagement triangle illustrating key geometric relationships in Proportional Navigation.

Figure 3.5 depicts the engagement triangle, showing the relative positions and velocity

vectors of the missile and target, as well as the Line-of-Sight (LOS) and range vectors. The LOS angle λ is defined with respect to the horizontal axis, δ denotes the lead angle. This collision triangle is fundamental to PN logic, as it characterizes the interception geometry and ensures that a properly guided missile can reach a non-accelerating target if the LOS rate is effectively controlled. While PN is effective against non-maneuvering targets, it lacks robustness when the target executes evasive maneuvers. To overcome the limitations of PN, Augmented Proportional Navigation (APN) incorporates the target's lateral acceleration a_T, improving accuracy against maneuvering threats. The APN formulation becomes:

$$a_{\text{aug}}(t) = N v_{cl} \dot{\lambda}(t) + 0.5 N a_T \tag{3.11}$$

where:

- N is the navigation ratio,
- v_{cl} is the missile-to-target closing velocity,
- $\dot{\lambda}(t)$ is the LOS rate, and
- a_T is the target's normal acceleration.

The additional acceleration term enhances interception performance by compensating for evasive maneuvers, reducing miss distance, and improving trajectory convergence [14].

Trajectory Tool Framework

The implementation of APN in this study follows an iterative computational scheme, illustrated in Figure 3.6. At each time step, the target's position and velocity are used to compute the LOS angle and required lateral acceleration. This acceleration is translated into a required lift coefficient C_L. If C_L exceeds the physically feasible maximum $C_{L_{\max}}$, the system saturates the lift and recomputes the physically achievable acceleration. The updated dynamics are then integrated to advance the pursuer's velocity, position, and pitch angle. The process continues until the closing distance no longer decreases, indicating either successful interception or loss of engagement feasibility. This framework ensures that trajectory corrections are continuously applied while adhering to aerodynamic constraints.

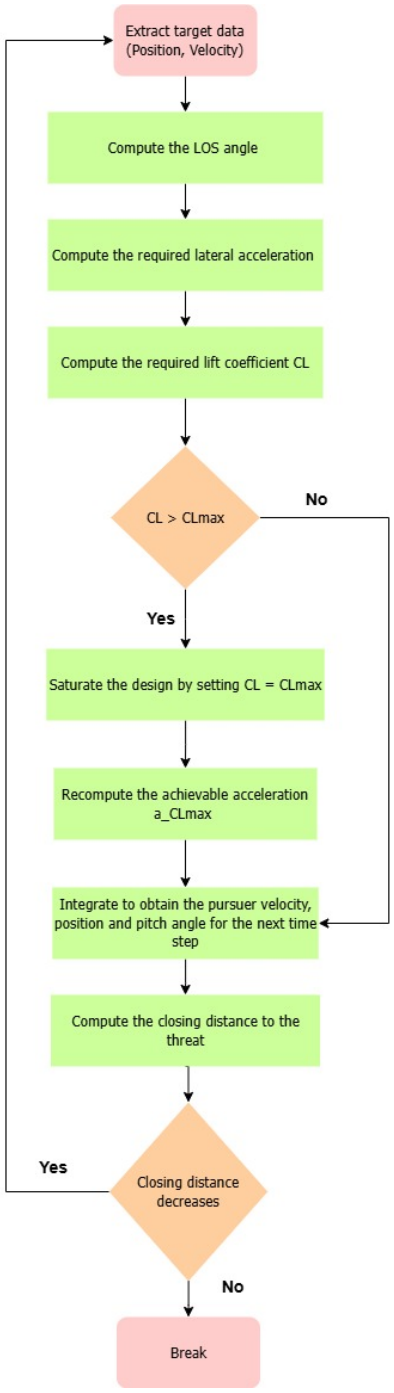

Figure 3.6: Flowchart illustrating the iterative implementation of Augmented Proportional Navigation in the trajectory simulation framework.

Guidance, Navigation, and Control System

The design of the guidance, navigation, and control (GNC) system is centered around a physics-informed implementation of Augmented Proportional Navigation (APN), integrated with real-time aerodynamic feedback for precise maneuvering. Threat tracking is enabled via a cost-effective conical scan semi-active radar seeker [15], which leverages the launch platform's radar for target illumination while requiring only a passive receiver onboard the missile—minimizing system complexity and cost while ensuring continuous line-of-sight (LOS) angle updates. These measurements feed directly into the APN algorithm, which computes the required lateral acceleration at each time step. This acceleration command is translated into a lift coefficient (C_L), retrieved through interpolation from a high-fidelity aerodynamic database indexed by Mach number and angle of attack. Fin deflection angles corresponding to the desired C_L are then determined. The control surfaces are actuated in real-time via high-bandwidth servomechanisms, ensuring the commanded deflection is achieved with minimal latency.

Crucially, the system is architected for immediate response: the onboard receiver remains powered in a low-energy listening mode during dormancy, allowing instantaneous threat detection, and the flight computer initializes trajectory computation and control logic within milliseconds. This enables the missile to transition from a dormant state to active boost-phase guidance in under one second, meeting stringent engagement timelines without compromising accuracy or control fidelity.

Seeker Noise Integration

To improve accuracy in trajectory simulation, the integration of seeker noise modeling was introduced. The primary objective is to enable a performance-cost trade-off by linking seeker-induced line-of-sight (LOS) error directly to seeker cost. This approach supports early-stage design decisions, ensuring that performance gains from high-end seekers justify their added cost — a critical consideration under strict budget constraints. A key challenge in developing this model is the lack of publicly available data correlating seeker cost with tracking accuracy. While inertial measurement units (IMUs) offer more accessible data, especially in terms of angular and acceleration-based error propagation, these are less relevant in scenarios where the seeker dominates terminal guidance behavior. To capture seeker-induced LOS error, a statistical model was developed using a Gaussian process with

a moving mean. Specifically, the error at each trajectory point is estimated by averaging the errors of the previous five points, with the sixth point drawn from a Gaussian distribution centered on that moving mean. The standard deviation of the distribution is then defined as a function of seeker cost, enabling a parametric sweep in trade studies. In parallel, a brief Gauss-Markov model was implemented for the IMU error profile. Combined with a low-pass filter, this allowed us to observe how accuracy improved as cost increased. The resulting curve made it clear that after a certain point, increasing IMU cost yielded minimal improvement in error reduction, effectively identifying the zone of diminishing returns. While seeker data is more limited, this modeling approach provided a reference framework to anticipate similar behavior for seeker performance versus cost. This noise integration method allows the simulation environment to reflect more realistic engagement outcomes and supports cost-optimized seeker selection within broader system-level design trade studies. The Figure 3.7 displays two possible trajectories for the engagement scenario.

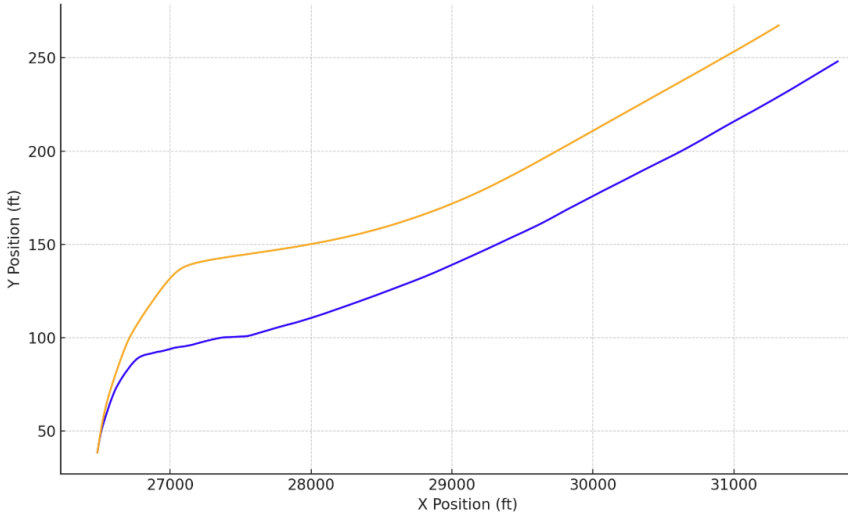

Figure 3.7: Pursuer Trajectory with Noise Modeling

Threat Stochastic Trajectory

To enhance realism and improve the accuracy of interception modeling, stochastic threat maneuvers were integrated into the simulation framework. Unlike deterministic paths, which assume threats fly predictable trajectories, the stochastic approach accounts for evasive behavior, particularly relevant in the final phase of engagement.

In this model, threats are allowed to maneuver at each simulation time step, but with

a probability that varies based on their proximity to the interceptor. Realistically, threats are unlikely to execute evasive maneuvers while far from the defended area or the incoming missile. Instead, the likelihood of maneuver increases as the relative distance between the missile and the threat decreases. To capture this behavior, maneuver initiation is modeled as a Bernoulli process, where the probability p of maneuvering is defined as a function of relative distance. This probability function is modeled using a normal distribution centered at 150 meters, representing the point at which evasive action becomes most likely. The farer the threat is from this point, the lower the chance it will maneuver. Once a maneuver is triggered, its aggressiveness is sampled within a range of 0 to 9 g's, consistent with the operational threat envelope specified in the Request for Proposal (RFP). The Figure 3.8 depicts 4 stochastic trajectories issued from the same Threat initial conditions. This probabilistic model allows the simulation to reflect more realistic threat behavior, enabling better evaluation of guidance robustness and overall system effectiveness.

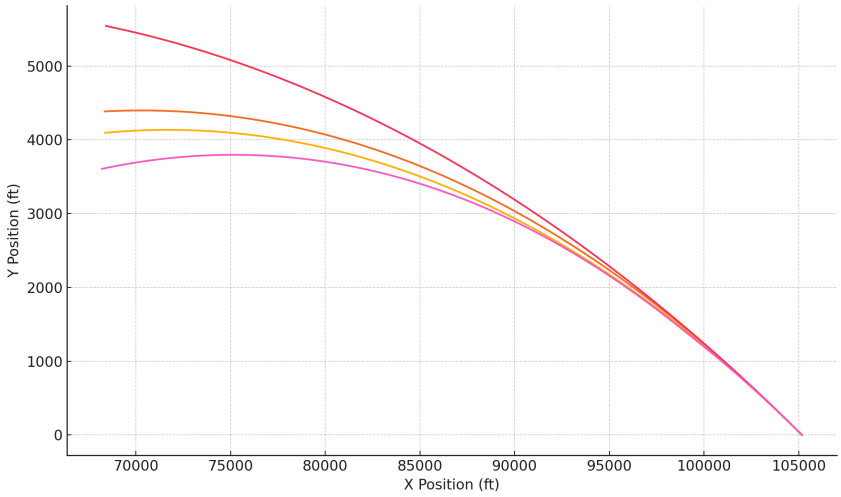

Figure 3.8: Stochastic Trajectory Sample for one Threat Scenario

Results of the Trajectory Integrator

Figure 3.9 illustrates three representative scenarios from a total of 7,000 simulated threat trajectories, all of which were successfully intercepted with a closing distance of approximately 0 meters. Each plot displays the trajectory of the threat (dashed red) and the corresponding pursuer path (solid blue), demonstrating the effectiveness of the implemented Augmented Proportional Navigation (APN) guidance law. The threats differ in their initial conditions, with variations in launch speed, starting location, and designated impact points within the

defense area, requiring the pursuer to adapt to a wide range of engagement geometries. The pursuer adapts dynamically to variations in the threat's motion, adjusting its trajectory to minimize miss distance. In some cases, initial corrective maneuvers are visible before the pursuer converges onto an optimal interception path, particularly when the threat follows a more complex or highly maneuverable trajectory.

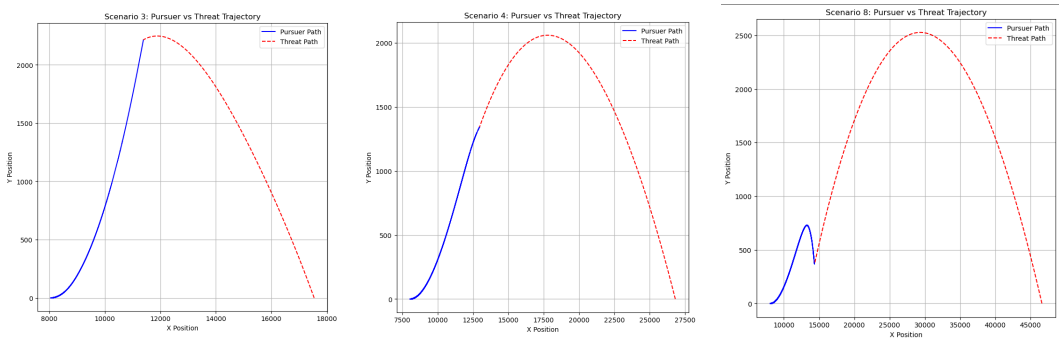

Figure 3.9: Comparison of different Proportional Navigation (PN) engagement scenarios.

3.3.3 Structures

As the structures subsystem is mostly driven by geometric parameters optimized to maximize the performance of the aerodynamic and propulsion subsystems, no initial design space exploration can be done, as the measures of effectiveness are not clearly defined. Having said that, the design space of the propulsion and aerodynamic system is defined based on measures of effectiveness that take into account multiple other parameters coming from the structures subsystems. This leads to an indirect design space exploration of the structure subsystems based on measures of merit from other subsystems.

To take into account the performance of the interceptor from a structures perspective in the final tool, the team is using two different tools to assess the mass properties and the loads the system can withstand. As the structure design variables are correlated with some design variables from the propulsion and aerodynamics subsystems, the following assumptions are made:

1. Body-Tube Diameter: The internal diameter of the body tube is driven by the external diameter of the casing of the motor. These two dimensions have to be the same.

2. Body-Tube Length: The sum of the length of the engine, the length of the nozzle,

and the thickness of the motor bulkhead must be less than or equal to the main body tube length.

3. General Geometric Dimensions: Most geometric dimensions (for example, the tip chord of the stabilizers and the control surfaces) are the same as the ones used in the performance analysis of aerodynamic subsystems.

Taking that into account, the team has automated the open source code *OpenRocket* [16] to run in batch mode in order to extract the following performance characteristics from the rocket, for multiple designs:

1. Center of Gravity vs time
2. Mass vs time
3. Moments of inertia vs time

As one can notice, the mass properties are all functions of time. This happens because the tool takes into account the mass flow rate of the engine. The engine properties, which are outputs of the propulsion subsystem, are included in the structures analysis through a RASP file created by our motor analysis tool (SMAC). Some early results of mass properties are presented in Figure 3.10.

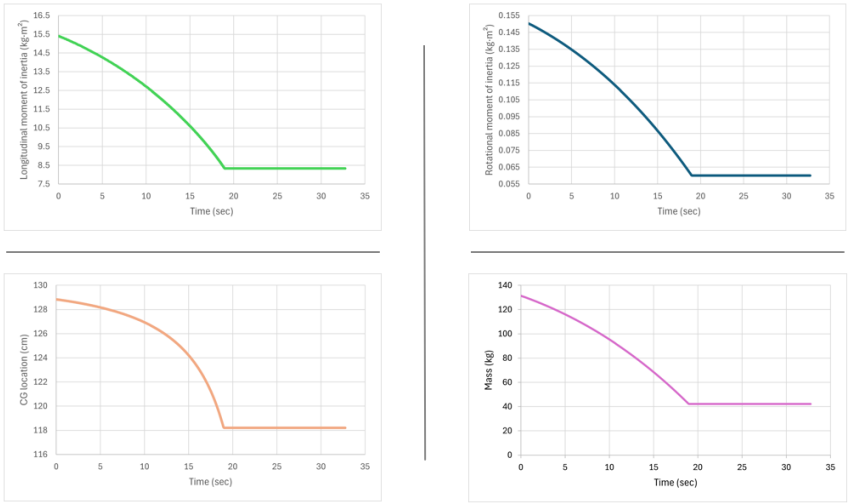

Figure 3.10: Mass Properties Over Time for a Notional Design. Top right: Rotational Moment of Inertia vs time, Top left: Longitudinal Moment of Inertia vs time, Bottom right: Mass vs time, Bottom left: Center of Gravity vs time

Finally, the last step concerning the structural analysis is the analysis of the loads the structure can take. Assuming that the loads are static and the interceptor is only subjected to bending and tension/compression, an in-house tool has been developed to check for different failure scenarios.

3.3.4 Propulsion

Solid rocket motors (SRMs) are widely used in ground-to-surface and low-cost systems applications due to their simplicity and long-term storage stability. For modeling the SRM in the ARROW project, an internal ASDL tool called the Solid Motor Development Code (SMAC) was utilized. SMAC enables users to modify various design, geometric, and propellant parameters to generate SRM specifications, including thrust and pressure curves, motor dimensions, and system weight. These outputs provide essential data for both trajectory and cost analysis.

SMAC operates by first defining the SRM geometry, which is then used as an input for a geometric burn simulation. The geometry module employs an edge-finding algorithm to converge on both nozzle and propellant geometries. The burn simulator subsequently models the combustion process using an unsteady lumped-parameter burn algorithm. An example of the burn simulation is illustrated in Figure 3.11.

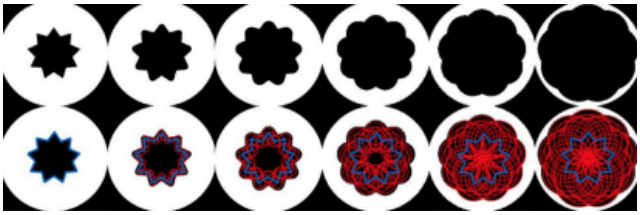

Figure 3.11: Example of SMAC's burn simulation [17]

Given the large number of input variables required for SMAC, a sensitivity analysis was conducted to identify the key parameters that significantly impact performance and cost. This analysis enabled a reduction in the dimensionality of the design space, improving computational efficiency without compromising accuracy.

Considering the short design range, low cost, and storage requirements, a BATES grain configuration was selected for further analysis. The Design of Experiments (DoE) variables for the propulsion subsystem are outlined in Table 3.5.

Table 3.5: DoE variable - Propulsion Subsystem

Variables	**Range**
Inner length (ft)	3.28 - 5.90
Inner diameter (in)	3.93 - 9.84
Diameter ratio	0.2 - 0.6
Maximum Expected Operating Pressure (psi)	300 - 1500
Propellant Type	discrete values

Regarding the propellant type, numerous formulations are available for solid rocket motors. Among these, three propellants—TP-H-1202, TP-H-3340, and TP-H-1148—were specifically highlighted in [18] due to the lack of publicly available information. For ease of reference, these propellants are respectively designated as Propellant A, B, and C.

3.3.5 Aerodynamics

As for the aerodynamic performance characteristics, the subsystem is again divided into two independent sections regarding design, but not performance: the control surfaces and the forebody. This leads to the challenging task of creating a performance assessment tool that can combine the effects of the control surfaces and the forebody at the same time, while their design spaces are mostly non-correlated. Each apparatus is going to be documented independently, and its effects are later going to be combined.

Control Surfaces

The control surface design space can be evaluated independently from the rest of the forebody regarding aerodynamics as the goals are fairly simply, maximize the effectiveness of the control surfaces regarding L/D and moment coefficients by minimizing weight and their effect on the stability characteristics of the rocket (don't move the center of pressure too much forward).

As the rocket might be able to reach speeds up to Mach 3, the team opted to use an open-source tool called *OpenVSP*. This tool was modified to use the vortex lattice method alongside the 2nd order Karman-Tsien Mach Number Correction scheme to account for compressibility corrections on subsonic to transonic aerodynamics coefficients [19]. This leads to a fairly accurate and quick tool ideal for conceptual design. Additionally, the tool

was modified to run batch cases of single control surface configurations and post-process the results to compute certain properties for optimized deflection angles of the control surfaces.

The post-processing starts by arranging the control surfaces around the interceptor's circumference based on their number, which is a design variable. The next step is to compute their effective angle of attack and sideslip angle for multiple deflection angles by taking into account a fixed angle of attack for the rocket and their placement angle. This procedure is purely mathematical, as the velocity vector is rotated around the control surface reference frame to match the inertial, based on the rotation matrices in the following equations, where θ_f is the fin placement angle around the body tube and α is the angle of attack of the vehicle.

$$R_{\text{wing frame}} = \begin{bmatrix} \cos\alpha & 0 & \sin\alpha \\ 0 & 1 & 0 \\ -\sin\alpha & 0 & \cos\alpha \end{bmatrix} \tag{3.12}$$

$$R_{\text{body frame}} = \begin{bmatrix} 1 & 0 & 0 \\ 0 & \cos\theta_f & \sin\theta_f \\ 0 & -\sin\theta_f & \cos\theta_f \end{bmatrix} \tag{3.13}$$

$$R_{\text{wing frame}} = R_{\text{body frame}} \cdot R_{\text{wing frame}} \tag{3.14}$$

After running the analysis for each fin at different interceptor angles of attack and Mach numbers, a matrix of coefficients is created and post-processed to represent the performance of each control surface on the interceptor's reference frame (common reference frame for every control surface). Next, the optimal deflection angle is selected for each fin based on the following scenarios:

1. Maximize C_L: Measure of effectiveness for maximum lift on a Rolling Airframe (RA) maneuver scenario.

2. Maximize CM_l: Measure of effectiveness for maximum rolling moment on a Rolling Airframe (RA) maneuver scenario.

3. Maximize C_L, while $CM_l = 0$: Measure of effectiveness for maximum lift on a Bank-To-Turn (BTT) maneuver scenario.

4. Maximize CM_l, while $C_L = 0$: Measure of effectiveness for maximum rolling moment on a Bank-To-Turn (BTT) maneuver scenario.

5. No effect, deflection angle = 0: Measure of effectiveness for minimum interference with stability and minimal drag.

Finally, their effects are summarized. The outputs of the aforementioned analysis provide insights into different areas of the design space based on multiple flight scenarios, like the interceptor's Mach number, the angle of attack, and the selected maneuver alternative scenario. One detail that must be pointed out here is that the weight of the control mechanism is estimated based on the hinge moment that is associated with a servo from online databases. The output file created for each control surface design, including their distance from the tip of the vehicle and the number of fins, provides the following information for each of the scenarios explained above.

1. Scenario where C_L is maximized: The control surfaces a fully deflected, without stalling, or deflected at a specific deflection angle to maximize their individual lift coefficient. The outputs for this case are the following:
   - C_{Lmax}/W
   - C_D/W, when C_L is maximized
   - $C.P.$, when C_L is maximized
   - C_{Ml}/W, when C_L is maximized
2. Scenario where C_{Ml} is maximized: The control surfaces a fully deflected in the same direction (clockwise), without stalling, to maximize their individual rolling moment coefficient. The outputs for this case are the following:
   - C_L/W, when C_{Ml} is maximized
   - C_D/W, when C_{Ml} is maximized
   - $C.P.$, when C_{Ml} is maximized
   - $C_{Ml}max/W$
3. Scenario where C_L is maximized, while C_{Ml} is almost zero: In this case, the code tries to identify the individual control surface deflection angles for which the overall lift of the vehicle is maximized but the rolling moment is close to zero. The reason this case shouldn't be confused with the first one is that when the interceptor is equipped with 3 control surfaces where the loads are not antisymmetric. The outputs for this case are the following:

- C_L/W, when C_L is maximized and C_{Ml} is close to zero
- C_D/W, when C_L is maximized and C_{Ml} is close to zero
- $C.P.$, when C_L is maximized and C_{Ml} is close to zero
- C_{Ml}/W when C_L is maximized and C_{Ml} is close to zero

4. Scenario where C_{Ml} is maximized, while C_L is almost zero: In this case, the code tries to identify the individual control surface deflection angles for which the overall lift of the vehicle is almost set to zero but the rolling moment is maximized. The same logic behind the antisymmetric aerodynamic loads is applied here. The outputs for this case are the following:

    - C_L/W, when C_L is almost zero and C_{Ml} is maximized
    - C_D/W, when C_L is almost zero and C_{Ml} is maximized
    - $C.P.$, when C_L is almost zero and C_{Ml} is maximized
    - C_{Ml}/W when C_L is almost zero and C_{Ml} is maximized

5. Scenario where the control surfaces are not deflected at all: In this case, the control surfaces are not deflected and are aligned with the body axis. This scenario is useful for predicting maximum speed and inertial characteristics. The outputs for this case are the following:

    - C_L/W, when the control surfaces are not deflected.
    - C_D/W, when the control surfaces are not deflected.
    - $C.P.$, when the control surfaces are not deflected.
    - C_{Ml}/W when C_L is almost zero and C_{Ml} is maximized

By the end of this step, the team can narrow down to a smaller design space and can decide to explore an area of the design space even more or shift towards analysis. In the latter case, the tool used for the control surfaces is the same. The change now is that the angle of attack and the Mach number are not noise variables but are default variables. This leads to the generation of multiple scenarios for each control surface set, while previously multiple control surface sets were investigated under randomly distributed flight scenarios to reveal statistics regardless of the flight scenario, meaning the combination of angles of attack and Mach numbers.

This time, the output of the analysis is a full aerodynamic deck for the control surfaces. An example of one of the five cases mentioned previously is shown here. In the actual csv file there are going to be four versions of it based on the four scenarios mentioned previously, maximizing C_L, maximizing C_{Ml}, maximizing C_L while C_{Ml} is close to zero, maximizing C_{Ml} while C_L is close to zero and zero deflection of the control surfaces.

1. For $AOA = i[deg]$ and $Mach = j$ The algorithm now computes the following values
    - C_L
    - C_D
    - C_N
    - C_A
    - C_{Ml}
    - $C.P.$
    - the deflection angle for each fin under that case

Forebody

Regarding the forebody, the selected tool to perform the performance analysis was RASAero. RASAero is a tool using semi-empirical methods to calculate the aerodynamic coefficients of supersonic or subsonic rockets. In our case, this particular tool was selected because of its accuracy in predicting certain stability characteristics of sounding rockets that other tools can't predict accurately. As for the design space, the same process was followed as before. By synchronizing RASAero with the mass estimation tool, the team was able to extract certain information regarding some measures of effectiveness regarding the aerodynamic properties of the forebody. The results of this tool provide the following aerodynamic parameters:

1. For each combination of AOA and $Mach$ number:
    - C_L
    - C_D
    - C_N
    - C_A
    - C_{Ml}

- *C.P.* defined as a distance from the tip of the interceptor

In this case, the Mach number and angle of attack are not noise variables but are used to define scenarios. This is done so that the team can directly discard interceptor designs whose aerodynamic performance suddenly drops under adverse angle of attack and Mach number scenarios. This could be done in the case of the control surfaces as the angle of attack was itself a function of the deflection of the surface, thus its optimal performance. This time, the outputs of proportional guidance provide insights that are directly relatable to the measures of effectiveness of the forebody, and this is why the angle of attack and Mach number are not noise variables anymore.

Regarding the Aerodynamic analysis of the forebody, a similar approach will be followed. The forebody's aerodynamic coefficients are to be determined again by using RASAero. The result will again be an aerodynamic coefficient deck for the rocket. The CN vs Mach number plot is seen in 3.12.

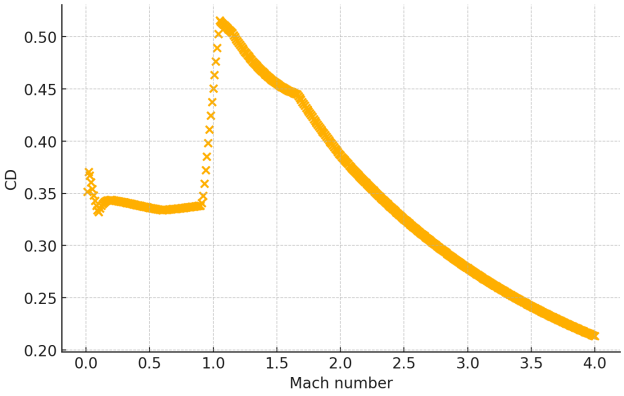

Figure 3.12: CN vs Mach Number

Integration

The final part of this stage is the integration of the aerodynamic properties by combining a set of control surfaces and a forebody for different Mach numbers, angles of attack, and deflection angles. Specifically, up to this point, for every control surface, a full matrix of aerodynamic coefficients based on deflection angle, Mach, and angle of attack for the forebody has been generated. Additionally, the same matrix is also created for the forebody. To create a combined aerodynamics deck that summarizes the effect of all the aforementioned components and provides a database of aerodynamic coefficients for the trajectory tool, the

effects of individual components must be combined and their interference must also be accounted for. First, the aerodynamic coefficients, $C_L, C_D, CM_l, X_{cp}, C_N$ for the control surfaces and the forebody are presented in the following section:

1. Aerodynamic Deck for Maximizing $C_{L_{cs}}$ (which is the lift coefficient for the control surfaces), regardless of what happens to CM_l (Rolling moment coefficient): Optimal scenario for Rolling Airframe maneuver alternative with a bias towards pitch maneuvers.

2. Aerodynamic Deck for Maximizing CM_l, regardless of what happens to $C_{L_{cs}}$: Optimal scenario for Rolling Airframe maneuver alternative with a bias towards roll maneuvers.

3. Aerodynamic Deck for Maximizing $C_{L_{cs}}$ while $CM_l = 0$: Optimal scenario for Bank to Turn maneuver alternative with a bias towards pitch maneuvers.

4. Aerodynamic Deck for Maximizing $CM_l = 0$ while $C_{L_{cs}} = 0$: Optimal scenario for Bank to Turn maneuver alternative with a bias towards roll maneuvers.

5. Zero Deflection of the Control Surfaces: Optimization towards stability and drag

At this point we have all the necessary information to start integrating the aerodynamic decks of the control surfaces and the forebody into one final table. To do that, we need to account for the interaction of these two. By using the aerodynamic correction factors proposed by Harlan Nelson and Derek Hillstrom, the body-fin interference is modeled as cited for highly supersonic missiles [20].

3.3.6 Secondary Subsystems

The remaining subsystems are mentioned as secondary subsystems because limited information can be provided for their design in the conceptual design phase. Both the Warhead and Avionics subsystems are heavily constrained by other design parameters that dictate the available volume. To that extent, the modeling of these subsystems is rather limited.

Warhead - Payload

Many assumptions are made for the warhead as a subsystem, with the major ones being: the presented area of the target (as specified by the RFP), the vulnerable area of the target

(assumed to be equal to the presented area for targets such as missiles), the type of warhead (a fragmentation 2D warhead with a toroidal spray pattern), and the metal mass to explosive charge ratio, which is taken to be 1.

The warhead neutralizes targets through two main mechanisms. The first is the pressure wave generated by the explosion, which causes damage at short range. The second is the damage inflicted by high-velocity fragments, which are embedded around the explosive and propelled outward at high speeds. The mean mass of each fragment is assumed to be 3.2 grams, and the energy per unit mass of the explosive (TNT) is 4,184 joules (J/g).

The modeling of the warhead is therefore entirely based on assumptions and follows the methodology proposed by Fleeman [10]. This methodology states that the probability of kill is a function of the miss distance and the ratio of explosive to fragment mass in the missile. Furthermore, the probability of kill for fragmentation warheads is maximized when this ratio equals 1. The single-sortie probability of kill is given by the following formula:

$$SSP_k = 1 - \left(1 - \frac{A_v}{A_p}\right)^{n_{hits}}, \quad n_{hits} = n_{fragments}\left[\frac{A_p}{2\pi \sin(\theta)\sigma^2}\right] \tag{3.15}$$

where A_v is the vulnerable area, A_p is the presented area, $n_{fragments}$ is the number of total fragments (based on the metal mass, which must be equal to the explosive mass), and both combined must equal the designed warhead mass.

The design process for the warhead can be divided into two parts: (1) determining the overall designed mass and volume of the warhead, and (2) calculating the probability of kill and arranging the warhead within the body tube.

3.3.7 Salvo Analysis

To explore cost-effective ways of achieving high missile defense performance, the team considered salvo analysis as a means to improve overall system effectiveness without relying solely on expensive, high-performance interceptors. In missile defense, the probability of kill increases when multiple interceptors are launched against a single target due to redundancy and overlapping engagement probabilities. This concept led the team to investigate whether firing multiple lower-cost missiles in a coordinated salvo could match or exceed the performance of a single high-cost missile at the same or lower total cost. To test this, missile designs were first generated without cost constraints to ensure a wide design space. Salvos of one, two, and three interceptors were evaluated based on a sensitivity analysis, which showed

that increasing beyond three interceptors results in minimal gain in cumulative probability of kill while sharply increasing cost. The Equation 3.16 depicts the overall probability of kill of a salvo, where n is the number of interceptors launched. Each configuration was assessed for total cost and resulting probability of kill. Results were plotted to generate a probability of kill versus cost curve, and a Pareto front was identified (see Figure 3.13). This approach allowed the team to compare different configurations and determine whether salvos of low-cost missiles offer a better cost-effectiveness profile than single high-cost units, providing a data-driven basis for design selection.

$$P_k = 1 - (1 - SSP_k)^n \tag{3.16}$$

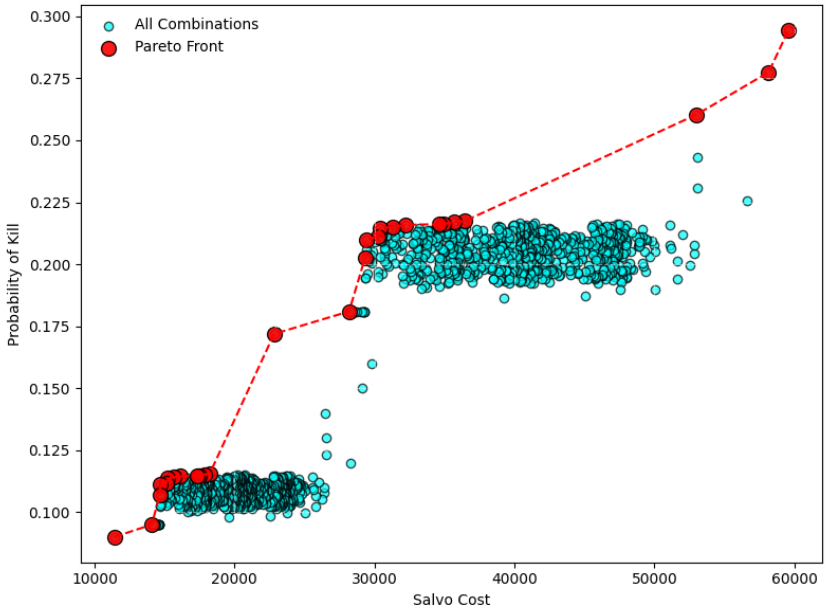

Figure 3.13: Salvo Analysis

Avionics

Finally, the avionics subsystem is even more difficult to identify thoroughly and numerically as it heavily depends on the operating environment, the threat, the launch platform, the support equipment, and the control subsystem. One major decision that was made before even going into the modeling of this subsystem is the type of guidance that the interceptor is going to be equipped with.

Laser guidance offers significant benefits for surface-to-air interceptor missiles, particu-

larly in terms of precision, resistance to electronic countermeasures, and the potential for passive target tracking. Unlike radar-guided systems, laser-guided interceptors can operate with reduced electromagnetic signatures, making them harder to detect and jam. Additionally, laser systems can provide pinpoint accuracy, which is especially advantageous when engaging small, agile, or low-signature targets such as cruise missiles or UAVs. However, incorporating laser guidance into an interceptor missile presents considerable challenges at the conceptual design stage. The effectiveness of laser guidance is highly dependent on atmospheric conditions, line-of-sight limitations, and precise alignment between the sensor and missile seeker, all of which introduce complex integration and operational constraints. Moreover, key parameters—such as the type of optical sensors, laser beam characteristics, stabilization systems, and target acquisition algorithms—are difficult to fully define early in the design process due to a lack of detailed data and the evolving nature of mission requirements. As a result, laser-guided systems often require iterative development and testing, making them harder to fully model and optimize during the initial conceptual phase [21].

To define the design space limits regarding guidance and avionics, the team decided to introduce an artificial error term that is directly associated with the cost of the unit. Again, the design considerations during this stage are related to the weight, the placement, and the volume of the avionics unit alongside its cost characteristics. Given a database that was created by the team, the cost of different laser guidance units was associated with the standard deviation of the error between the actual and the measured line of sight. Next, a Gaussian distribution was assigned to this error for every timestep, and 1000 samples were taken to find the mean of this error per timestep. Finally, the used line of sight for the trajectory algorithm is the mean of the actual line of sight plus the error for the last 1000 measurements.

Chapter 4

Optimization By Parameters Variation

Designing a cost-effective anti-missile interceptor requires navigating a fundamental trade-off: minimizing production cost while maximizing probability of kill (Pk). This chapter details how a multi-objective evolutionary optimization framework (NSGA-II) was implemented to explore critical design parameters, ranging from warhead mass to sensor bandwidth, and to generate a Pareto front of optimal trade-offs. The process integrates existing cost, structure, propulsion, and trajectory analysis tools into a closed-loop optimization environment.

4.1 XDSM

The implemented integrated simulation workflow provides a modular framework for evaluating missile performance by linking trajectory, propulsion, structures, and cost. Built entirely in Python, the framework was driven by the NSGA-II evolutionary algorithm, chosen for its ability to efficiently explore non-linear, multi-objective design spaces without relying on gradient information. Its strength in handling mixed variable types and maintaining solution diversity made it particularly well-suited for optimizing across both performance and cost metrics.

To reduce the computational load, particularly from aerodynamic simulations involving control surface modeling, aerodynamic data are precomputed and held constant throughout

the optimization. Each candidate design instead pulls from a stored aerodynamic dataset, allowing the loop to focus its computational resources on the dynamic elements of the simulation—guidance logic. This implies that the geometric features of the design could not be iterated.

This setup enables fast and consistent evaluation of candidate designs while retaining high-fidelity aerodynamic influences. Cost and probabilistic kill modeling feed into the optimizer to assess trade-offs across hundreds of potential configurations.

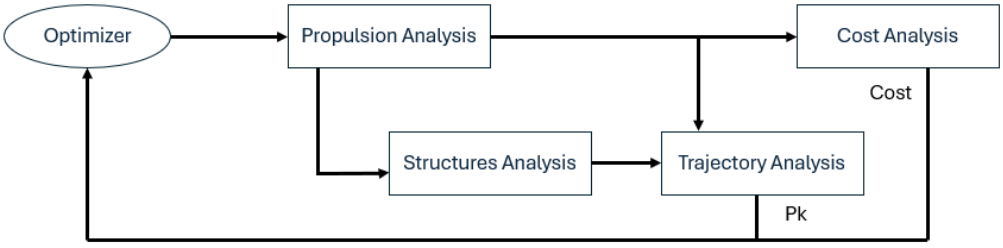

Figure 4.1: XDSM Diagram

4.1.1 Optimization Formulation

As we cannot change geometric features, only specific design variables related to propulsion, lethality, and avionics can be iterated. These variables are presented in Table 4.1. Allowing adjustments to motor characteristics and avionics cost/error enables a more comprehensive search for the optimal design.

Table 4.1: Design variables for optimization

Variable	Range / Choices
Warhead Mass (lbm)	11–19
MEOP (psi)	550–800
Inner Ratio	0.095–0.300
Propellant Type	A, B, or C
Angular Bias Instability (°/hr)	2.0–10.0
Acceleration Bias Instability (µg)	2.2–30.0
Acceleration Bandwidth (Hz)	225–750
Angular Bandwidth (Hz)	250–550

4.1.2 Optimization Implementation

Our optimization loop is built on the Non-Dominated Sorting Genetic Algorithm II (NSGA-II), which seamlessly balances competing objectives and preserves solution diversity without requiring gradient information. NSGA-II commences by randomly sampling an initial population of 20 candidate designs from the defined parameter ranges. Each design was evaluated end-to-end, and its parameters were updated in the baseline model. The production cost is computed via a cost analysis tool, enabled by the SME, and the intercept performance (probability of kill) is estimated through the trajectory integrator and probabilistic engagement model. Once all candidates are assessed, NSGA-II ranks solutions by Pareto dominance—non-dominated designs forming the first front, those dominated only by first-front members forming the second, etc., and computes a crowding distance metric within each front to estimate the local solution density. Parents are selected via a binary tournament, prioritizing lower Pareto rank and larger crowding distance, and then bred through simulated binary crossover and polynomial mutation (for continuous variables) and uniform crossover (for categorical variables). The resulting offspring merge with the parent population, and the combined pool is resorted to yield the next generation's top 20 individuals. This generational loop was repeated for 250 trials (approximately five generations), steadily advancing the Pareto front.

Within this context, the Pareto front itself represents the envelope of optimal trade-offs between the cost and kill probability, where each point corresponds to a design for which no other candidate is strictly better in both objectives. Moving along the front illustrates the inherent trade-off —achieving a lower cost requires accepting reduced intercept effectiveness, and vice versa. This continuous frontier equips the Team with a spectrum of viable designs, enabling selection of the balance between affordability and lethality that best aligns with operational priorities.

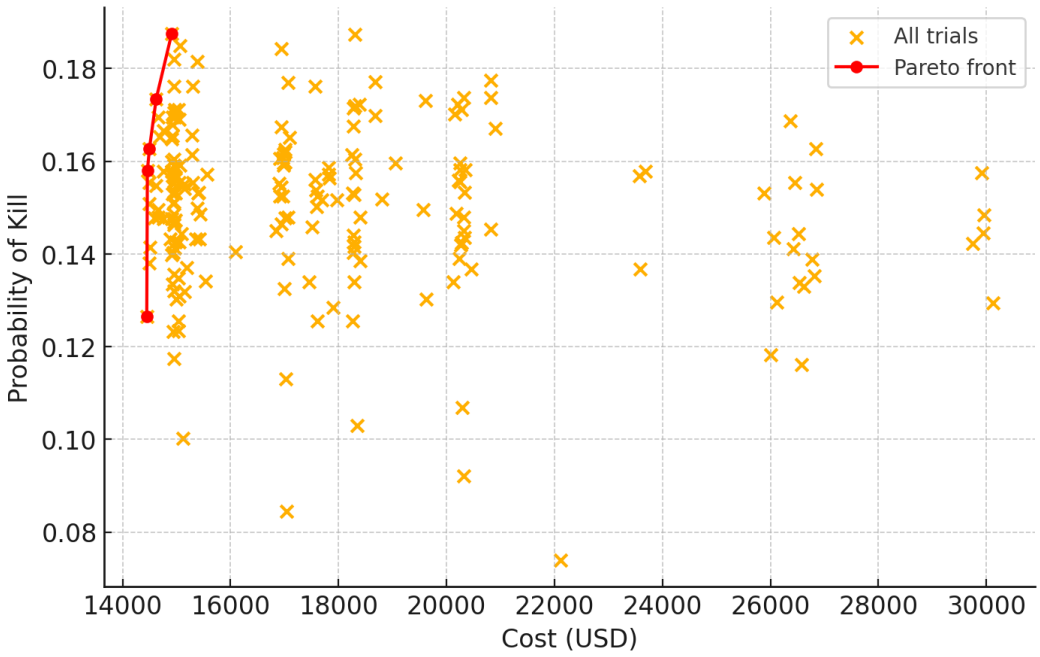

Figure 4.2: Optimization sample results

Chapter 5

Final Design

In this section of the report, the final design is presented alongside some of the results generated by the aerodynamics, propulsion, structures, trajectory, and cost tools. Next, some validation calculations are presented. Finally, the collaboration and interface between specific subsystems related to guidance and control will be accounted for before the preliminary design of the control mechanism and subsystems.

5.1 Design Parameters

5.2 Drawings

The following figure, 5.1, presents a section view of the project arrow based on the available space for every subsystem as defined by the aforementioned processes of filtering, down selection, and optimization. Starting from the nosecone tip and moving down, the subsystems illustrated are the avionics (blue and yellow volumes), the avionics-warhead bulkhead (dark red), the warhead (red volume), the control mechanism and the supporting motor bulkhead (dark blue and dark red volumes), the control surfaces (dark green fins), the engine (gray volume) and finally the stabilizers (light green and gray surfaces). Another 2D view, which stresses the placement and presence of the support structures, is presented in 5.2. As can be seen, there are additionally the Avionics-Warhead bulkhead, the motor bulkhead, and the motor retainer that bolt the internal components to the external supporting structure.

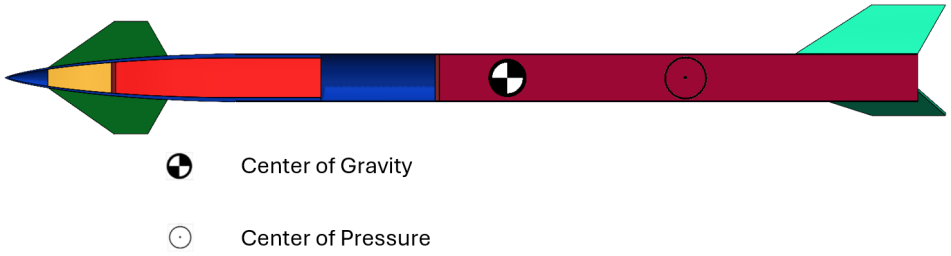

Figure 5.1: Section view of project ARROW

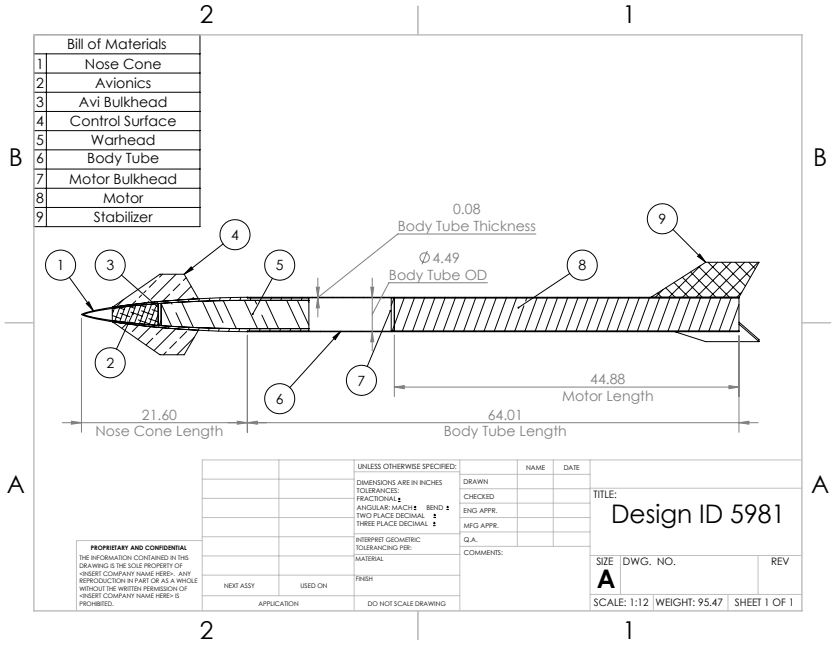

Figure 5.2: Section view of project ARROW

Figure 5.3 is helpful in understanding the importance and distribution of internally arranged elements. As can be seen, the majority of the internal volume and mass are distributed between the warhead-payload subsystem and the propulsion subsystem.

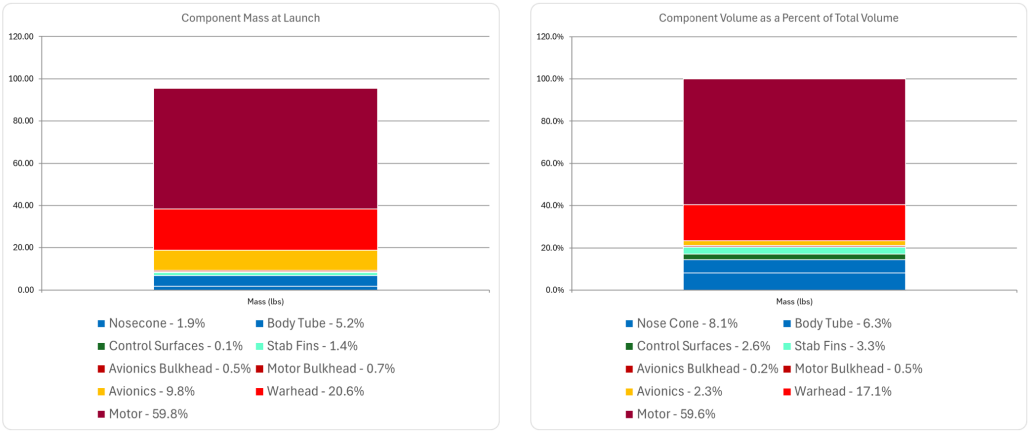

Figure 5.3: Stacked bar charts of the components' weight and volume

5.3 Performance Results

Aerodynamic Properties

The geometric properties of the surfaces contributing to the aerodynamic characteristics are presented in Table 5.1. These were selected through the previously mentioned section of design space exploration and filtering. Contrary to some other subsystems, these geometric properties do not propagate into the optimization tool and are fixed from that point on for the baseline vehicle, and thus constrain the final optimized design.

In the following paragraphs, some geometrical properties will be presented for the control surfaces, the nosecone, and the stabilizers, alongside some manufacturing techniques and structural characteristics.

Structural Characteristics For clarity, some additional details of the previously mentioned components are highlighted in this section. These details are very helpful when trying to explain the structure of some components during the manufacturing process. The nosecone and the body tube are made out of fiberglass and carbon fiber composites. More detail will be given in the following section, as their structural details are less important than other subsystems. The control surfaces and stabilizers are made out of sandwich composites. A soft metal core is created before carbon fiber-epoxy layers are glued on top of it. AS a result, the component is solid and inherits both the structural properties of the carbon fiber (endurance under thermal and structural static loads) and the properties of

Table 5.1: Geometric Characteristics of Aerodynamic Components

Variable	CM_{ZERO}
Nosecone Diameter	4.48 $[in]$
Nosecone Length	21.57 $[in]$
Body-Tube Length	65.15 $[in]$
Control Surface Number	4
Control Surface Root Chord	9.21 $[in]$
Control Surface Tip Chord	3.13 $[in]$
Control Surface Semispan	1.78 $[in]$
Control Surface Sweep Angle	55 $[deg]$
Control Surface Distance from the Tip	5.9 $[in]$
Control Surface Total thickness	0.2 $[in]$
Stabilizers Number	3
Stabilizers Root Chord	11.45 $[in]$
Stabilizers Tip Chord	6.92 $[in]$
Stabilizers Semispan	4.52 $[in]$
Stabilizers Sweep Angle	57 $[deg]$
Stabilizers Distance from the Tip	75.27 $[in]$
Stabilizers Total thickness	0.3$[in]$

the aluminum core (makes it less prone to flutter, as the core is softer).

Manufacturing Processes The manufacturing processes used to materialize the previously mentioned components can be divided into two categories; Layered or Sandwiched structures.

1. Sandwiched Structures: The manufacturing process of a sandwich-structured composite fin with an aluminum core and external carbon fiber layers involves combining materials to leverage both strength and lightweight properties. The aluminum core must first be surface-treated through cleaning and abrasion to ensure strong adhesion. Carbon fiber layers—typically in prepreg form—are laid over both sides of the aluminum, with fiber orientations chosen based on load requirements. These layers are then bonded using either co-curing, where all components are cured together in a vacuum bag inside an autoclave if one is available. After curing, the fin is trimmed, drilled, and inspected for defects using methods like ultrasonic testing.

2. Layered Structures: The winding or prepreg process for manufacturing carbon fiber and fiberglass composite structures like the nosecone and the body tube involves precision-controlled methods to produce high-strength, lightweight components. In the winding process, continuous fibers—either carbon or fiberglass—are impregnated

with resin (wet winding) or come pre-impregnated (prepreg tow), and are wound under tension onto a rotating mandrel in specific patterns, such as helical or hoop, to meet structural load requirements. Once the desired layup is complete, the part is cured, typically in an oven or autoclave, and then removed from the mandrel. In the prepreg process, sheets of fiber pre-impregnated with resin are manually or automatically laid onto molds in layered sequences, with precise control over fiber orientation. These laminates are then vacuum-bagged and cured under heat and pressure to achieve a void-free, consolidated structure. In our case, the cost-effectiveness of prepregs makes them the more reasonable choice.

Aerodynamic Results As for the aerodynamic properties of the final selected system, a drag polar will be presented for the control surfaces, along with a CN vs. Mach diagram at different angles of attack for the forebody in Figure 5.4.

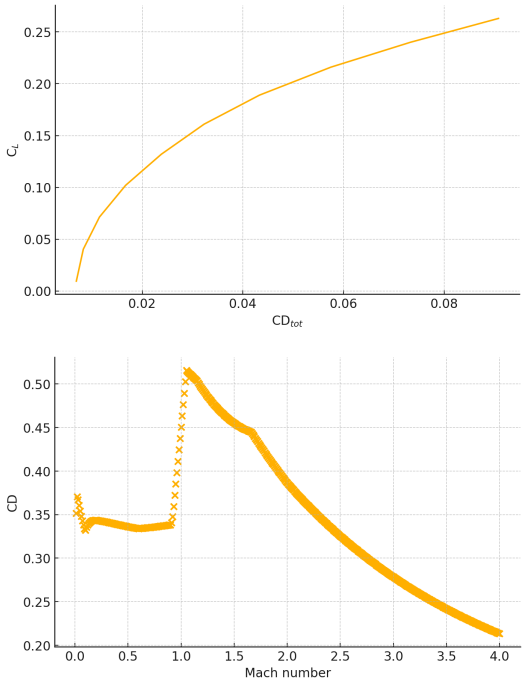

Figure 5.4: CL vs. $C_{D,\text{tot}}$ and C_N vs. Mach number.

As mentioned previously, the information extracted from these two tools is later combined, and interaction effects are accounted for to simulate the overall impact of these components on the aerodynamic performance of the vehicle.

Finally, a chart including this type of information at selected points for zero angle of

Table 5.2: Aerodynamic Coefficients for Various Angles of Attack and Mach Numbers

Scenarios	CL_{ZERO}	CD_{ZERO}	$C.P._{ZERO}$	CM_{ZERO}
Angle of Attack = 0°, Mach number = 0.1	0.000	0.45	1.62	0
Angle of Attack = 4°, Mach number = 0.1	0.68	0.5	1.422	1.71
Angle of Attack = 8°, Mach number = 0.1	1.36	0.64	1.426	3.43
Angle of Attack = 12°, Mach number = 0.1	2.02	0.88	1.428	5.17
Angle of Attack = 15°, Mach number = 0.1	2.48	1.12	1.43	-6.49
Scenarios	CL_{max}	CD	$C.P$	CM
Angle of Attack = 0°, Mach number = 0.1	0.97	1.45	0.35	7.38
Angle of Attack = 4°, Mach number = 0.1	1.53	1.61	0.75	4.78
Angle of Attack = 8°, Mach number = 0.1	2.11	1.51	0.96	2.43
Angle of Attack = 12°, Mach number = 0.1	2.67	1.85	1.08	-0.07
Angle of Attack = 15°, Mach number = 0.1	3.06	2.15	1.14	-2.07

attack of the control surfaces and max angle of attack (before stall) for the control surfaces is presented in Table 5.2. One important aspect of the aerodynamic parameter deck is that the trajectory algorithm, given an angle of attack and a Mach number for each timestep, interpolates between aerodynamic values (as they follow a linear pattern for small angle of attack) to calculate the required deflection angle of the control surfaces. This is done in order to achieve the desired lift or drag force, which originates from the lateral and longitudinal accelerations computed by the proportional guidance code. Another important aspect is the stability of the vehicle. As can be seen from the last column of table 5.2 and for the scenario where the control surfaces are fully deflected, the pitching moment coefficient is positive for small angles of attack, which indicates instability. Thus, the algorithm also limits the deflection of the control surfaces to maintain a stability margin greater than 1.4 at all times during flight.

5.3.1 Propulsion Properties

The propulsion characteristics of the finalized missile configuration were obtained using the Solid Motor Analysis Code (SMAC). The design parameters of the SRM of ARROW

are outlined in the Table 5.3. Key parameters of interest, such as total impulse, specific impulse, or burn time, are summarized in Table 5.4. These values reflect the optimized design outputs based on mission requirements and system constraints. Additionally, the thrust profile generated by SMAC is shown in Figure 5.5, illustrating the thrust curve over the duration of the burn. This plot highlights the expected performance envelope, including the peak thrust and the steady-state behavior of the motor, which are critical for accurate trajectory prediction and overall system performance.

Variable	Value
MEOP (psi)	599.46
Inner ratio	0.231
Propellant Type	B
Grain type	Bates

Table 5.3: Design Parameters of ARROW's SRM

Variable	Value
Burn Time (s)	9.1
Mean Thrust (lbf)	1,201
Max Thrust (lbf)	2,717
Total Impulse (lbf.s)	11,061
Propellant Mass (lbm)	41.89
Motor Mass Pre-launch (lbm)	57.09

Table 5.4: Propulsion Characteristics of the final design ARROW

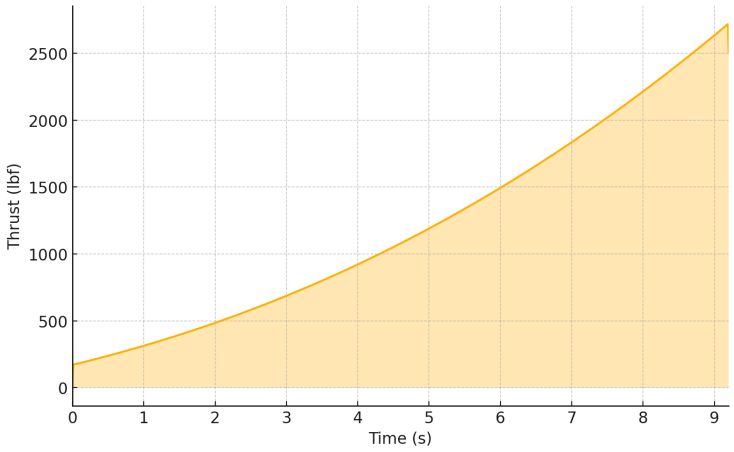

Figure 5.5: Thrust Curve of ARROW

5.3.2 Structural Properties

Weight Breakdown In the following table, 5.5 the weight breakdown of the selected design is presented. The detail of each component is limited as many coupling schemes have not yet been decided, and some electrical and control mechanisms are not finalized.

Table 5.5: Weight Breakdown of Project ARROW

Component	**Weight [lbm]**	**Percent of Launch Mass [%]**
Nosecone	1.83	1.8
Body Tube	4.93	5.05
Control Surfaces and Servos	2.13	2.15
Stabilizers	1.35	1.3
Avionics Bulkhead	0.45	0.4
Motor Bulkhead	0.68	0.7
Avionics	9.36	9.6
Warhead	19.64	20.3
Motor (Pre-launch)	57.09	58.7

Aero-thermal Heating Environment As the missile is capable of reaching speeds exceeding Mach 3, placing the vehicle in the upper supersonic regime, it is deemed necessary to conduct an aero-thermal study to define the capabilities of the vehicle. To assess the effects of these phenomena, the team decided to conduct high-fidelity CFD analysis based on the worst-case scenario for the most affected parts of the missile, using the ANSYS suite.

The first step is to identify the components under extreme heating stresses. Based on open literature, [22], [23] the components that are subjected the most to heating stresses are the nosecone, the leading edges of the control surfaces and the leading edges of the stabilizers. Additionally it is mentioned that the heat transfer is more intense when multiple shocks overlap over a surfaces. To validate this assumption, the team simulated a symmetry plane at Mach 3 to visualize the formation of possible shock waves, and the results are presented in Figure 5.6.

Figure 5.6: Whole Missile Mach Contour

As can be seen, three major shock waves are forming on the vehicle at Mach 3. These shock waves are formed at the tip of the nosecone and the leading edges of the control surfaces and the stabilizers. Another interesting aspect is that the nosecone shockwave and the control surface shockwave overlap with each other, creating a double point, which is expected to be the place of maximum enthalpy rise. This means that individual analysis of every component is not sufficient, and thus the nosecone and the control surfaces must be analyzed together, and the stabilizers alone.

Starting with the nosecone and the control surfaces, the team opted for an axisymmetric 2D analysis as the geometry is simple enough to assume radially uniform flow at zero angle of attack. To account for the worst-case scenario and keep computational cost to a minimum, the analysis conducted was steady state, with no heat transfer between the flow and the body, leading to adiabatic conditions when the system will reach equilibrium (non-realistic). The spatially discretized domain can be seen in Figure 5.7, where it is also apparent that the created mesh is almost perfectly structured, as can be cross-checked by the skewness and aspect ratio distribution of the elements in Figure 5.8.

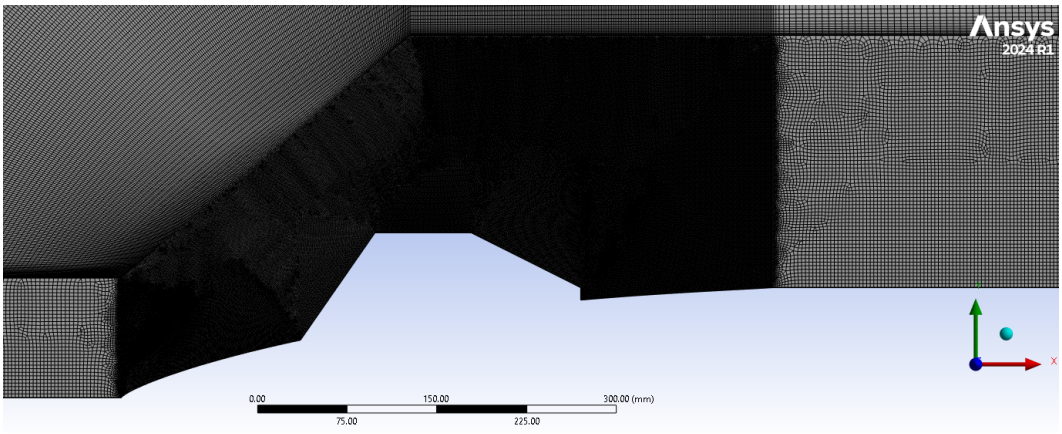

Figure 5.7: Nosecone & Control Surfaces Computational Domain Discretization

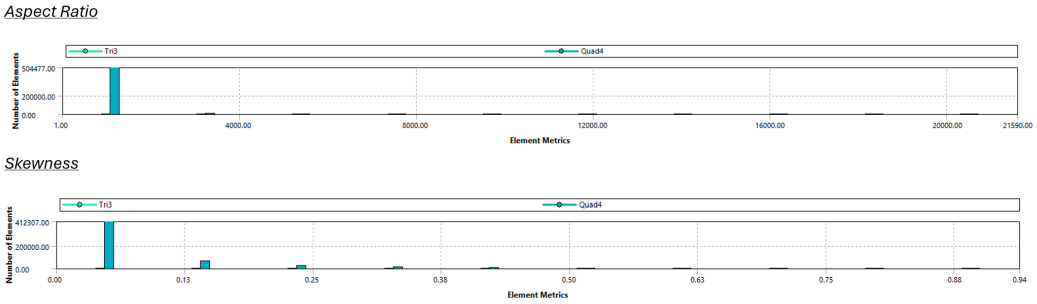

Figure 5.8: Skewness & Aspect Ratio Distribution

Moving on to the setup and solution part, the selected turbulence model was k-omega SST in order to avoid using wall functions and resolve the viscous boundary layer to some extend, which is responsible for a percentage of thermal heating. This leads to a targeted y+, lower than 1, which will be evaluated later on. Finally, to simulate the worst case scenario, the thermal boundary condition for the wall was set to adiabatic wall, which translates to no diffusion; coupling that with the steady state scenario, we are simulating an occasion where the thermal heating cannot be dissipated towards the inside of the nosecone and thermal equilibrium is reached on the outside. Finally, a contour plot of the temperature and a line plot of the surface temperature on the nosecone and the control surfaces are presented in figures 5.9 and 5.10, respectively.

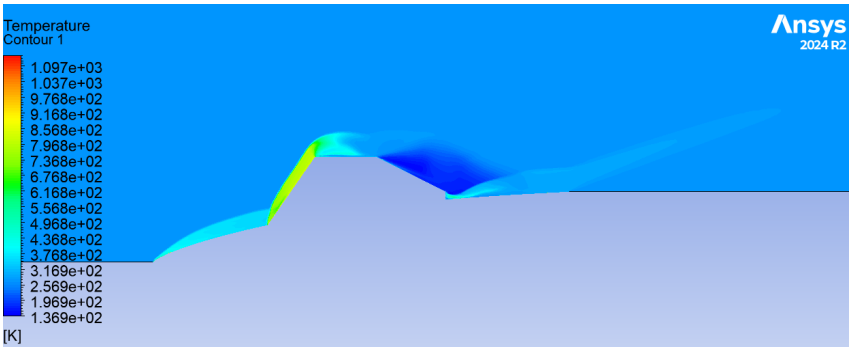

Figure 5.9: Nosecone Tip Temperature Contour Plot

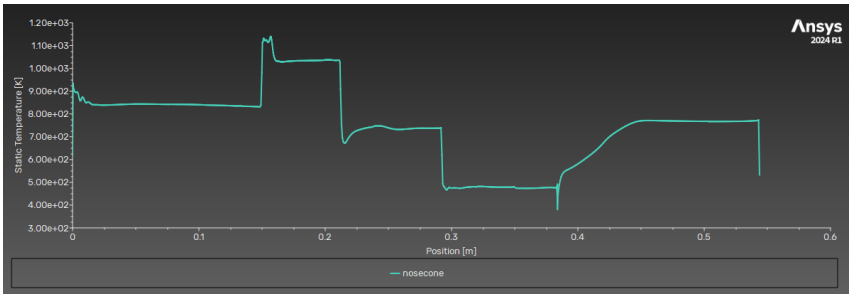

Figure 5.10: Nosecone Surface Temperature Distribution.

Finally, the wall Y+ was also plotted to validate the spatial discretization, where the residuals in figures 5.12 and 5.11 respectively. The material selected for the construction of the nosecone, *D-Glass Fiber Glass*, is both RF transparent (with a dielectric constant of 4.1 and a dissipation factor of 0.001 at 1 GHz) and can withstand the calculated maximum temperature (up to 1133.15 K) without any degradation of it's structural properties. The control surfaces are made out of carbon fiber, on the other hand, and as we can see, the maximum temperature is encountered near the leading edge and close to the root of the fins. The material selected for this area is a carbon-carbon composite with an aluminum core.

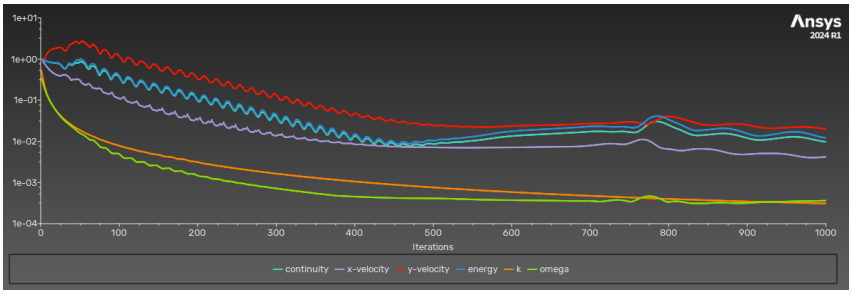

Figure 5.11: Nosecone CFD Analysis Residuals

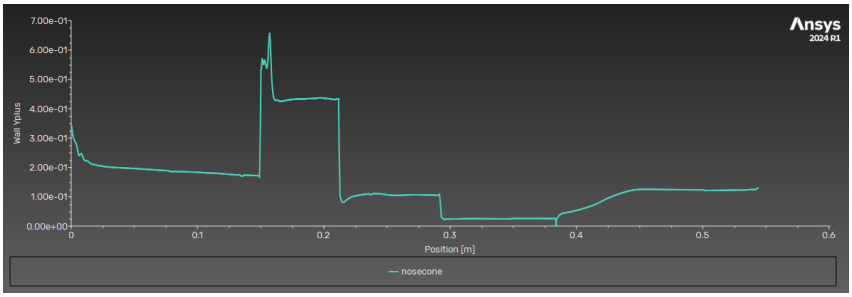

Figure 5.12: Nosecone Analysis Actual Wall y+

Moving on to the stabilizers, the same approach is followed. Firstly, the mesh qualities can be seen in Figure 5.13. By using the same setup, the residuals and the contour of the calculated wall Y+ are presented in Figure 5.14. Finally, the temperature contour of that area and the temperature profile are also presented in Figure 5.15. As can be seen, these are experiences with significantly lower thermal stress, as there is just one shock wave impinging on the leading edge.

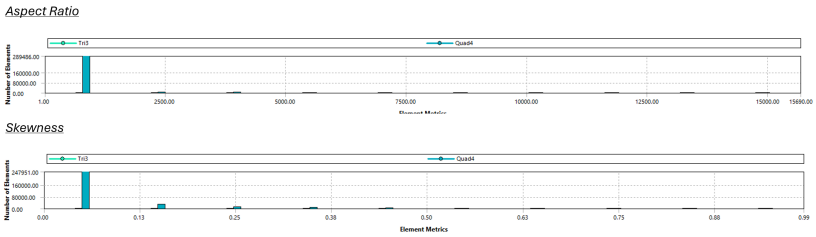

Figure 5.13: Stabilizers Mesh Qualities

Wall Y+

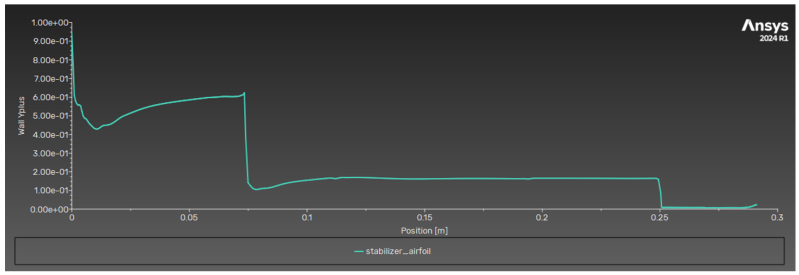

Residuals

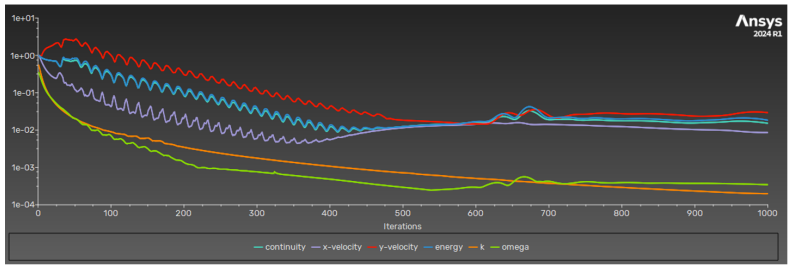

Figure 5.14: Stabilizers Solution Metrics

Temperature Contour

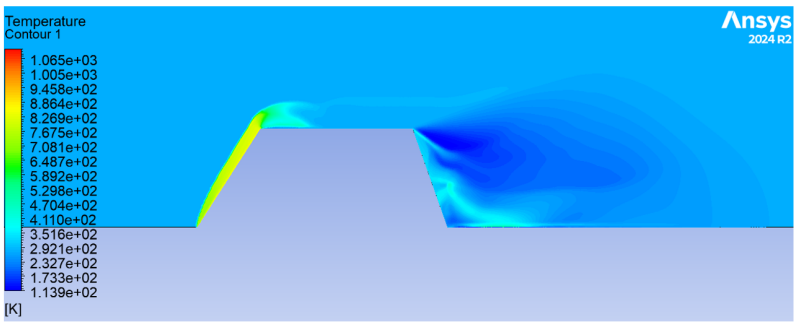

Temperature Profile

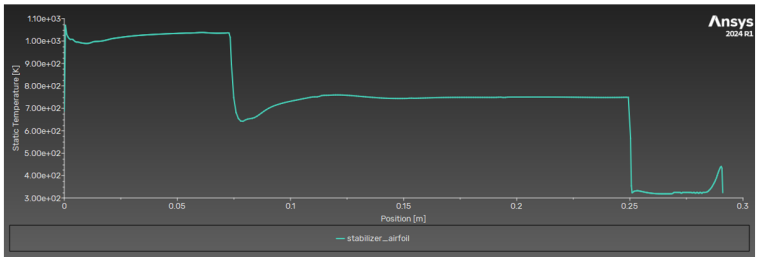

Figure 5.15: Temperature Contour and Profile along the Stabilizer's L.E.

5.4 Interception Scenarios

In order to efficiently assess the performance of ARROW, thousands of missile interceptions were generated.

5.4.1 Single Sortie Probability of Kill - SSPK

The single-shot probability of kill (SSPK) for the final missile design, ARROW, was assessed through a two-phase simulation campaign. In the first phase, ARROW, along with all other designs, was tested against a focused set of 120 threat scenarios representing the most challenging targets, defined by the Request for Proposal (RFP) as threats with minimum maximum Mach numbers between 2.5 and 3 and time-to-intercept windows ranging from 15 to 35 seconds. The probability of kill distribution for ARROW is depicted in the Figure 5.16. This subset of 120 threat scenarios was selected to balance fidelity with computational efficiency while ensuring coverage of the worst-case performance envelope. Against this high-speed, short-reaction-time subset, ARROW achieved an overall SSPK of 15%. In the second phase, ARROW was launched against the full space threat envelope consisting of 2,000 scenarios, encompassing a broader range of targets with minimum and maximum Mach numbers of 0.5 to 3, thus including both typical and worst-case threats (see Figure 5.17 for the probability of kill distribution). In this full-spectrum analysis, the overall SSPK increased to 49%, demonstrating ARROW's effectiveness across a diverse threat landscape.

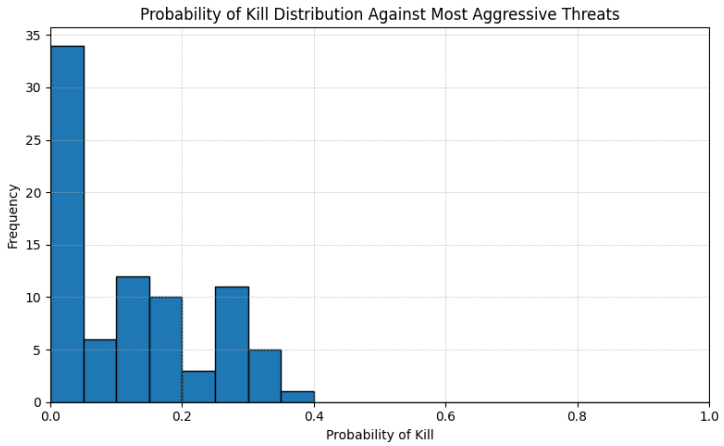

Figure 5.16: Probability of Kill Distribution for Worst Threat Scenarios

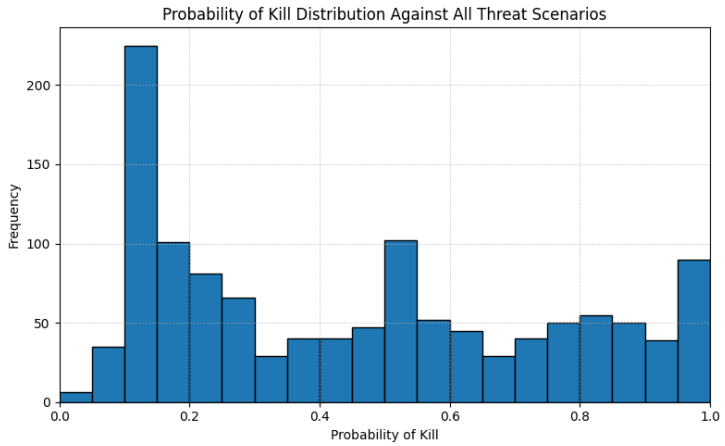

Figure 5.17: Probability of Kill Distribution for All Threat Scenarios

5.4.2 Salvo Scenarios

To evaluate the operational effectiveness of the ARROW system beyond single-shot scenarios, a salvo engagement analysis was conducted. Launching multiple interceptors can significantly improve the probability of kill against challenging threats. While a three-unit salvo was considered, the marginal gain in Pk did not justify the substantial increase in cost and complexity. Therefore, a two-unit salvo was selected as the most practical trade-off. Figure 5.18 presents the updated Pk distribution under this salvo configuration against the entire threat envelope. With two ARROW interceptors launched per threat scenario, the overall Pk increases from 49% to 64.1%, marking a significant improvement in engagement reliability while maintaining system affordability and logistical feasibility.

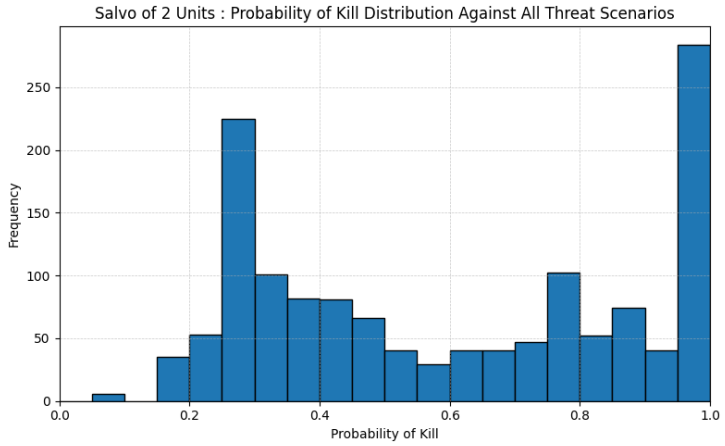

Figure 5.18: Salvo of 2 Units: Probability of Kill Distribution for All Threat Scenarios

5.5 Time history

Time history data for both the interceptor and threat trajectories are presented in the following subsections. The interceptor dataset includes altitude, range, velocity, Mach number, and additional flight performance parameters such as the variation of missile weight, thrust over time, and propellant mass flow rate $\dot{m}$, as well as the fin deflection angles for Fin 1 and Fin 3 in degrees. Since the current simulation is restricted to two-dimensional motion and controls only pitch dynamics, only two opposing fins (Fin 1 and Fin 3) are actively used for guidance and maneuvering. The threat data includes altitude, range, velocity, and Mach number. These trajectories are used to assess compliance with the performance requirements. In addition to the tabulated data, the closing distance plot in Figure 5.19 illustrates the relative motion between the interceptor and the threat over time, showing a reduction in separation distance that converges to zero at the point of interception.

5.5.1 Threat

Table 5.6: Trajectory Data Over Time

Time	X (ft)	Y (ft)	V (ft/s)	Mach
0.00	61,685.29	0.00	2,756.17	2.47
0.50	60,313.45	100.99	2,746.21	2.46
1.00	58,945.76	193.65	2,737.26	2.45
1.50	57,581.76	278.02	2,729.24	2.45
2.00	56,221.09	354.14	2,722.04	2.44
2.50	54,863.45	422.06	2,715.43	2.43
3.00	53,508.66	481.80	2,709.10	2.43
3.50	52,156.50	533.38	2,703.04	2.42
4.00	50,806.89	576.81	2,697.36	2.42
4.50	49,459.90	612.10	2,691.87	2.41
5.00	48,115.61	639.29	2,686.39	2.41
5.50	46,774.11	658.38	2,680.82	2.40
6.00	45,435.51	669.40	2,675.05	2.40
6.50	44,099.92	672.36	2,668.99	2.39
7.00	42,767.47	667.28	2,662.60	2.39
7.50	41,438.28	654.20	2,655.87	2.38
8.00	40,112.51	633.12	2,648.79	2.37
8.50	38,790.29	604.08	2,641.43	2.37
9.00	37,471.79	567.09	2,633.81	2.36
9.50	36,157.19	522.19	2,626.07	2.35
10.00	34,846.66	469.38	2,618.31	2.35
10.50	33,540.40	408.71	2,610.68	2.34
11.00	32,238.59	340.19	2,603.34	2.33

5.5.2 Pursuer

Table 5.7: Interceptor Trajectory and Performance Parameters

Time	X(ft)	Y(ft)	V(ft/s)	LOS(deg)	a_lat	a_long	CL	CD	CM	Xcp(ft)	CN	Mach	Weight(lbf)	Thrust(lbf)	$\dot{m}$ (lbm/s)	AOA(deg)	Fin1	Fin3
0.00	26,484.25	0.00	0.00	0.00	0.00	0.00	0.00	0.00	0.00	0.00	0.00	0.00	0.00	0.00	0.00	0.00	0.00	0.00
1.00	26,484.25	38.55	132.74	45.05	-39.41	59.27	25.49	1.12	-6.49	4.70	2.69	0.12	66.13	193.11	1.34	28.32	0.00	0.00
1.50	26,550.18	65.05	153.38	47.33	-35.59	59.34	16.01	1.12	-6.49	4.70	2.69	0.14	62.82	199.79	1.57	16.56	0.00	0.00
2.00	26,631.19	84.56	179.45	49.48	-5.52	43.03	9.69	0.91	-5.32	4.69	2.22	0.16	59.51	206.53	1.84	12.34	0.00	0.00
2.50	26,723.26	101.63	197.33	51.52	-20.04	65.92	7.21	1.37	-11.98	13.03	0.49	0.18	56.16	213.35	2.13	8.04	-57.61	57.61
3.00	26,829.13	114.55	227.94	52.32	-3.57	52.33	5.73	1.16	-8.95	4.00	0.43	0.20	54.23	220.24	2.44	6.35	-43.48	43.48
3.50	26,948.66	127.15	252.17	52.99	-8.38	43.06	5.33	1.05	-7.48	1.18	0.40	0.23	52.36	227.19	2.78	5.53	-36.30	36.30
4.00	27,079.42	137.11	275.29	54.14	-37.54	74.14	5.14	0.63	-2.47	3.01	0.33	0.25	49.82	234.22	3.15	2.71	-9.91	9.91
4.50	27,227.08	140.83	315.42	56.92	-1.16	83.36	4.02	0.61	0.68	4.62	0.31	0.28	45.21	241.31	3.54	0.93	9.01	0.00
5.00	27,394.60	143.06	354.65	60.30	2.82	81.46	2.76	0.65	1.09	4.48	0.31	0.32	39.78	248.48	3.96	0.70	11.53	0.00
5.50	27,581.72	145.17	394.36	63.98	0.94	81.73	1.51	0.65	1.14	4.46	0.31	0.35	33.99	255.72	4.41	0.67	11.82	0.00
6.00	27,789.12	147.53	435.98	67.85	-1.08	83.58	0.65	0.64	1.09	4.48	0.31	0.39	28.03	263.02	4.89	0.70	11.53	0.00
6.50	28,018.04	150.46	480.43	71.83	0.43	89.46	0.33	0.63	0.94	4.53	0.31	0.43	22.11	270.40	5.41	0.78	10.64	0.00
7.00	28,270.29	154.37	529.20	75.73	6.19	102.64	0.39	0.59	0.62	4.64	0.31	0.47	16.53	277.85	5.95	0.97	8.62	0.00
7.50	28,548.43	159.87	584.37	79.10	10.59	122.12	0.44	0.54	-0.06	4.86	0.31	0.52	11.88	285.37	6.52	1.27	4.75	0.00
8.00	28,856.04	167.62	648.25	80.68	11.52	140.47	0.26	0.49	-1.01	5.07	0.31	0.58	9.38	292.97	7.13	1.59	-0.66	0.66
8.50	29,198.22	178.41	724.34	78.61	19.26	166.03	0.05	0.62	-2.20	4.47	0.32	0.65	10.35	300.63	7.76	2.01	-7.43	7.43
9.00	29,582.69	193.31	817.25	69.90	17.07	196.62	0.09	0.75	-3.39	4.21	0.33	0.73	17.72	308.37	8.43	2.37	-14.83	14.83
9.50	30,017.29	211.64	925.17	53.07	5.84	235.00	0.30	0.85	-4.16	4.94	0.34	0.83	31.04	316.18	9.14	2.44	-20.35	20.35
10.00	30,510.20	232.47	1051.64	27.13	9.11	274.93	0.33	0.91	-4.30	5.74	0.34	0.94	46.19	324.06	3.86	2.40	-23.36	23.36
10.50	31,071.82	256.38	1202.37	-8.00	26.36	329.34	0.21	1.00	-4.51	6.59	0.34	1.07	51.77	332.02	0.00	2.48	-29.30	29.30
11.00	31,318.86	267.36	1271.88	0.00	22.67	365.39	0.22	1.02	-4.79	6.97	0.35	1.14	47.15	335.22	0.00	2.59	-32.31	32.31

5.5.3 Closing Distance Over Time

As the interceptor and threat proceed along their respective trajectories, the time histories presented in **??** and 5.7 provide key performance metrics for both. At each time step, the closing distance between the two is continuously computed, and Proportional Navigation (PN) is applied to minimize the line-of-sight (LOS) rate. The interceptor commands lateral acceleration to reduce this angular rate, guiding it toward the target. As a result, the closing distance steadily decreases and ultimately approaches zero, indicating a successful interception, as can be seen in Figure 5.19.

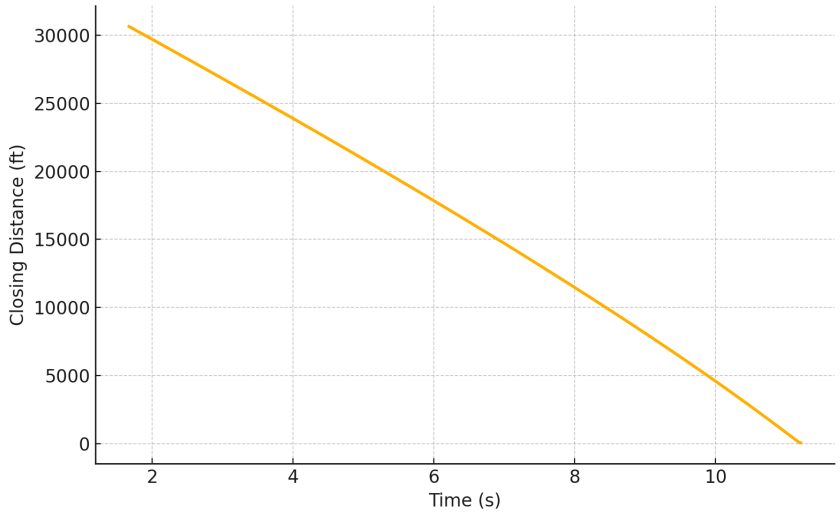

Figure 5.19: Closing distance between interceptor and threat over time

5.6 Cost-Performance Trade-off

The cost-performance trade-off analysis was conducted through parameter variation optimization, as detailed in Chapter 4. This systematic analysis successfully identified the Pareto front (illustrated in Figure 5.20), highlighting the optimal design that maximizes performance while minimizing cost. Consequently, the probability of kill against the most aggressive threats was significantly improved from 11% to 15%, with only a modest cost increase of 3.6%. The specific characteristics of the ARROW missile before and after the parameters variation are outlined in Table 5.8.

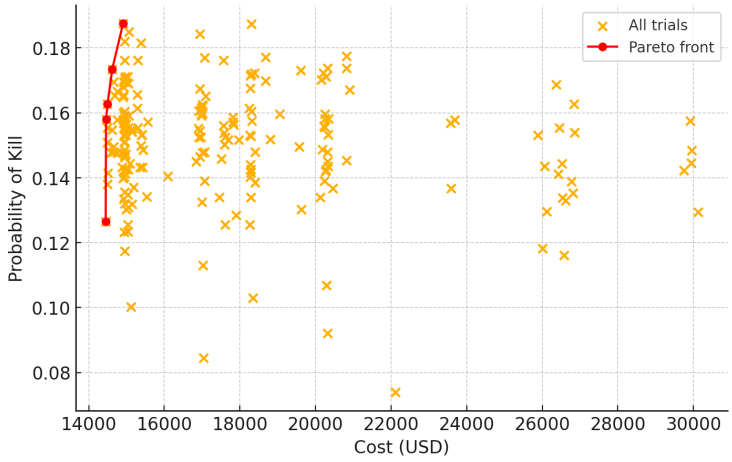

Figure 5.20: Optimization Trials

Variable	Parameters Before Variation	Parameters After Variation
Propellant Type	B	B
meop (psi)	321	599
Inner Ratio	0.281	0.231
Acceleration bandwidth (Hz)	503.1	489.5
Angular bandwidth (Hz)	537.5	394.4
Acceleration Bias Instability (microgram)	27.28	12.87
Angular Bias Instability (deg/hr)	3.98	4.36
Warhead Mass (lbm)	26.21	19.62
SRM Cost (USD)	3891.29	4304.28
Seeker Cost (USD)	3256.21	4113.54
Total Cost (USD)	13,090.68	13,562.53
Probability of kill	0.11	0.15

Table 5.8: Results of the Parameters Variation

5.7 Cost Results

5.7.1 First Unit Production Cost

The tool, MCDAT, allows for the computation of the first unit production cost for the selected final design. Before applying the learning curve and taking into account the assembly and test, ARROW costs $ 16,122 per unit.

5.7.2 Mean Production Cost over 10 years

After applying the learning curve to the design, the cost of one interceptor drops to $ 13,563. The learning curve factor is set to 0.8 to balance between a labor-intensive learning curve and a machine-intensive learning curve.

5.7.3 Cost Breakdown

The tool, MCDAT, also outputs the cost breakdown of ARROW. This breakdown gives the repartition of the price of the different subsystems and allows to visualize the main drivers that influence the production cost (figure 5.21).

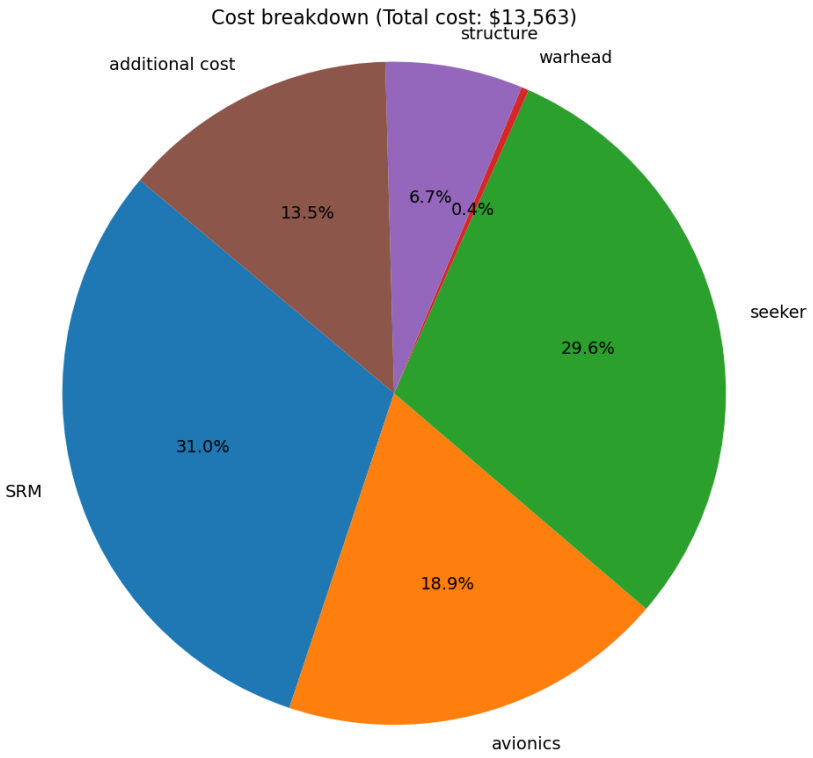

Figure 5.21: Cost breakdown of ARROW

As represented in Figure 5.21, the solid rocket motor and the seekers are the most expensive parts of the interceptor. They account respectively for 31 % and 29.6 % of the total cost. The avionics also has a large contribution (18.9 % of the total cost). The propulsion, as well as the electronic components and sensors, are the more technologically advanced systems in the interceptor, and they therefore drive the cost. In addition, the structure (which includes the aerodynamic subsystem), the warhead, and the additional subsystems are responsible for the remaining cost (20.6 % of the total cost).

5.7.4 Uncertainty Intervals

Uncertainty quantification is also performed to obtain an uncertainty distribution for the cost of the final design.

For the uncertainty regarding the cost of the structure and aerodynamic subsystem, a minimum, mean, and maximum value are computed using, respectively, the minimum, mean, and maximum price of the materials over the past 20 years. Then, a PERT probability distribution is assumed to obtain the distribution of the cost for the final design. The results

obtained are presented in Figure 5.22.

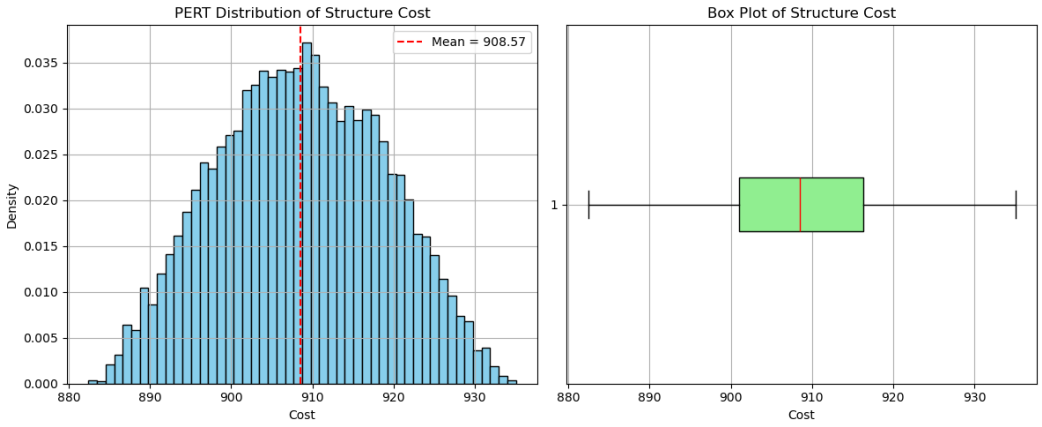

Figure 5.22: Uncertainty distribution for the structure subsystems (including the aerodynamics components)

Uncertainty quantification is also performed for the solid rocket motor and the IMU cost using a bootstrapping-based approach. For both of these components, 200 surrogates are trained by resampling the original dataset with replacement (as explained in the section 3.2.3). The uncertainty distribution obtained for the final design ARROW is represented in Figure 5.23.

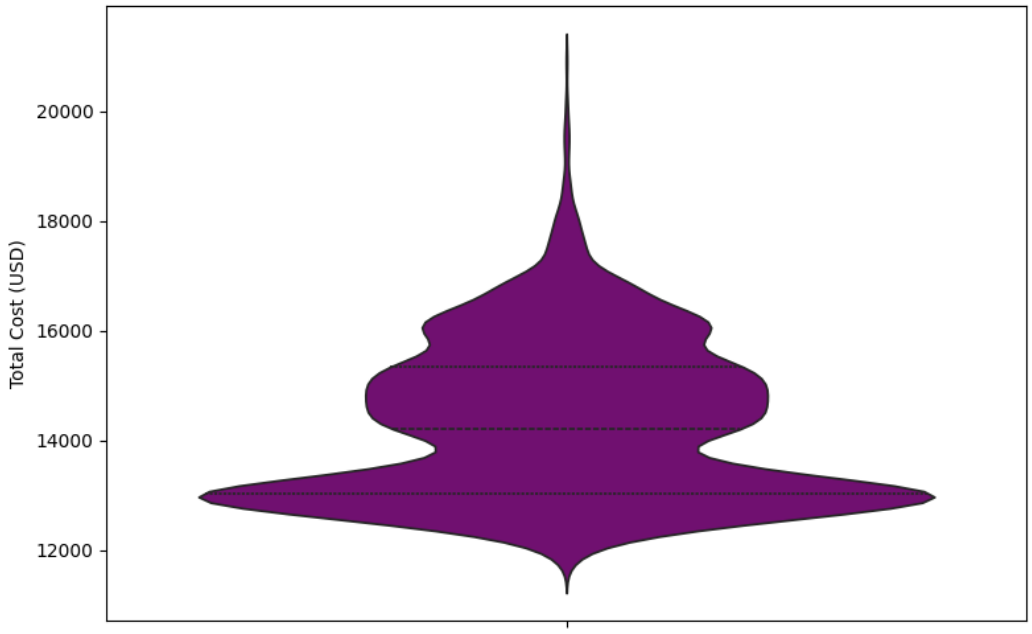

Figure 5.23: Uncertainty Distribution for ARROW's Cost

Finally, from this distribution, the 90% confidence interval is as follows : [$12,524.49 ; $ 16,761.98].

5.7.5 Life Cycle Cost

The life cycle cost is divided into several parts. It takes into account the acquisition cost, the operating cost, the support cost (corresponding to maintenance), and the RDT&E cost. The life cycle duration of ARROW is set to 30 years.

Using equation 3.5, we can estimate the RDT&E cost for the final design. This cost amounts to $ 74,642,643 and represents 18.3 % of the total LLC.

The acquisition cost is obtained by multiplying the mean production cost over 10 years by the number of units produced.

$$\text{Acquisition Cost} = \text{Mean Production Cost} \times \text{Number of units produced} \tag{5.1}$$

As mentioned in the RFP, 10,000 missiles should be produced for a period of 10 years, therefore, the number of units is set to 10,000 for the entire life cycle. Finally, the acquisition cost amounts to $ 135,625,305.

For the support cost (maintenance cost), an estimate of the preventive and of corrective maintenance costs is obtained for the final design. The preventive maintenance cost is obtained using equation 3.6. For the corrective maintenance that happens every 10 years, the cost depends on the type and the number of subsystems that should be replaced. A Monte-Carlo simulation across the 30-year life cycle is performed as explained previously. This simulation takes into account:

- Probability of failure per 4-month period and subsystem
- Cost of replacing each subsystem
- Likelihood of multiple component failures per event, sampled using a truncated normal distribution

Each simulation run computes the expected cost of corrective maintenance events. The results of the Monte-Carlo are presented in Figure .

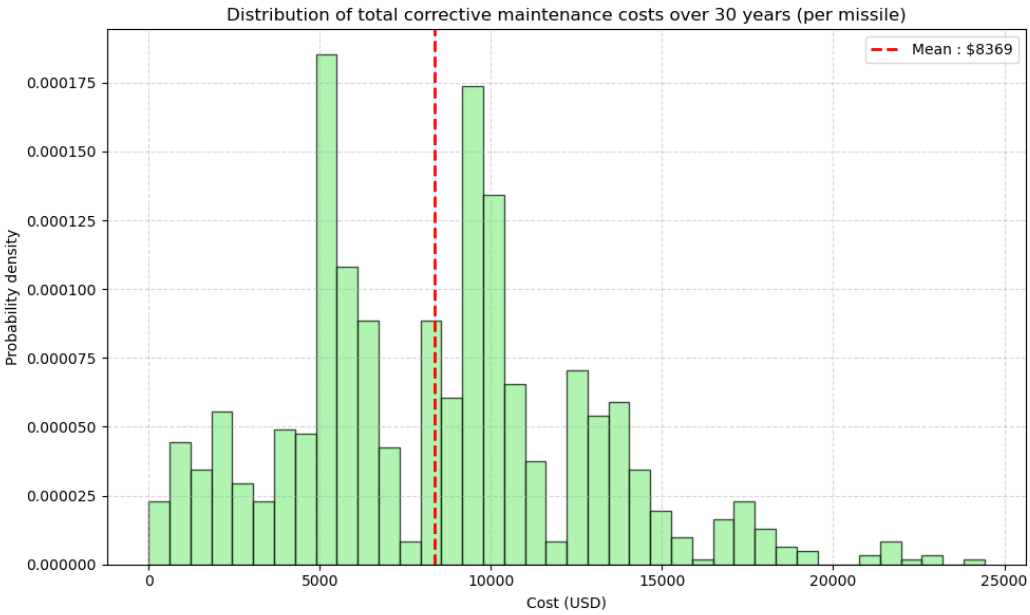

Figure 5.24: Corrective maintenance Monte Carlo simulation

By averaging the results across all the iterations, the cost of the corrective maintenance is determined. For the final design, the total maintenance cost (preventive and corrective added together) amounts to $ 173,566,490 for the whole life cycle.

Operating cost is computed using equations 3.7 and 3.8. The result obtained is $ 23,363,104 for the entire life cycle of the interceptor. The final life cycle cost breakdown is presented in Figure 5.25.

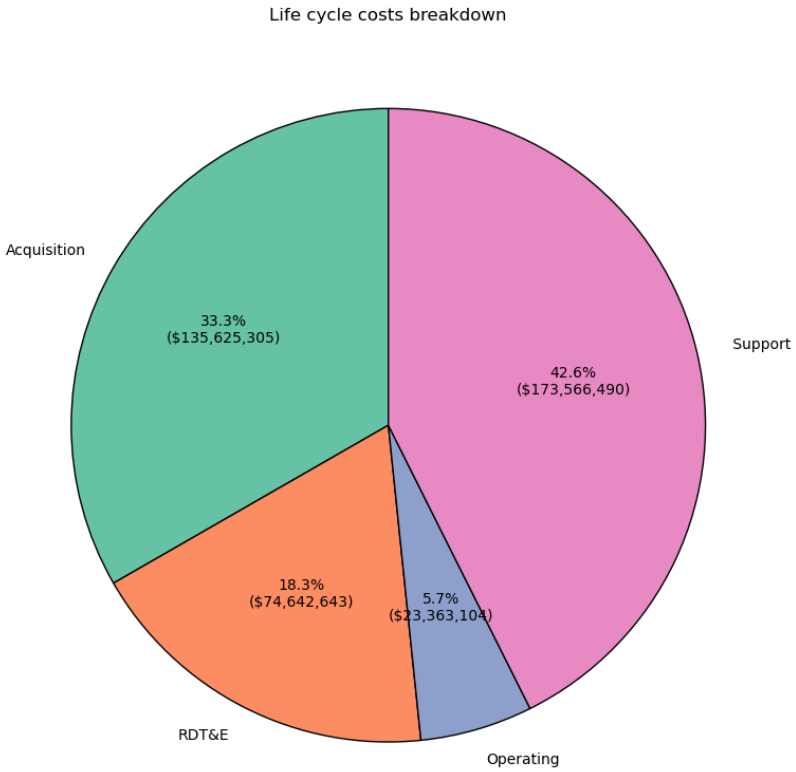

Figure 5.25: Life Cycle Cost breakdown of ARROW

Finally, an estimation of the overhead cost is computed using the following equation [24]:

$$\text{Overhead Cost} = 0.13 \times \text{Operating Cost} \tag{5.2}$$

Therefore, the overhead cost amounts to $3,037,203 for the final design ARROW.

5.7.6 Manufacturing and technology options to lower the cost

In order to further reduce the cost of production of the interceptor, several manufacturing and technology options can be considered and applied.

First of all, for the electronic components, the seekers, the sensors, and even the solid rocket motor, COTS components should be privileged. Using Commercial Off-The-Shelf systems reduces both development time and acquisition costs while enabling faster upgrades. Therefore, COTS components can maximize affordability, simplify supply chains, and accelerate development cycles, all while retaining sufficient reliability for the interceptor.

For the structure and the aerodynamic components, additive manufacturing (commonly known as 3D printing) could be an envisaged solution. In fact, this technology allows the creation of relatively complex geometries in a single build process. Thus, it is eliminating the need for multiple parts and costly tooling typically required in traditional manufacturing methods. This reduction in part count and assembly time ultimately leads to lower labor costs and fewer potential points of failure. For the aerodynamic surfaces, for instance, fins and control surfaces, additive manufacturing enables rapid prototyping. In addition, it allows on-demand production. These features can significantly shorten the development cycle and drastically reduce the overhead cost. Finally, the usage of the material is optimized when using additive manufacturing processes. The amount of waste is minimized, and therefore it generates savings. In brief, additive manufacturing makes it possible to produce structurally efficient components while reducing the overall production cost [25].

5.8 Development Plan

The development plan is outlined in a five-step approach to ensure successful progression from concept to final production. The first phase, Conceptual Design, is the initial design phase where many components are roughly designed and major design choices are made, leading to a limitation in future design freedom during preliminary and detailed design. One of these choices, which is described in previous sections, is whether some components are going to be bought (COTS) or designed and manufactured in-house. As for the in-house developed components, they must be adequately defined and sized as was done in previous sections of the report. Both the in-house and commercially available components are going to be listed in the table 5.9. This is followed by Development Testing, explaining the testing conducted to verify that the individual components and interfacing components perform as expected. The next phase, System Evaluation and Validation, will be a full system assessment to confirm that the integration of subsystems meets operational requirements while undergoing a simulation and testing of realistic conditions. Once the system has been validated, Initial Operational Capability will begin with a low-rate missile roll-out. Finally, in the Full-Rate Production phase, manufacturing will increase to full capacity and mass production.

In-house components and COTS components In the case of this system, the team is trying to minimize cost by acquiring different components from different sources. Some components, though, can't be purchased from external providers and have to either be manufactured and designed by the entity of interest or by an external associate. For example, the manufacturing difficulty and the cost of the equipment that is associated with graphite nozzles are big enough to drive the decision to outsource this particular component, while the technical difficulty of designing an IMU for our specific needs mandated that we use a commercially available one to keep the cost to a minimum. On the other hand, the design and manufacturing of some components of the motor, like the grains, is easy enough that it can be done in-house to cut down on expenses.

Component	Commercially Purchased or Developed in-house
Nosecone	In-House or Outsourced
Body Tube & stabilizers	Commercially Bought or Outsourced
Control Surfaces	In-House
Control Surface Mechanism	In-House
Control Surface Actuators	Commercially Bought
Avionics Bay	In-House
Avionics Hardware	Outsourced or Commercially Bought
Avionics bulkhead	In-house
Warhead & Fuse	In-house or Outsourced
Motor Bulkhead	In-house or Outsourced
Motor Retainer	In-house or Outsourced
Motor Casing	In-house or Outsourced
Motor Grains	In-house
Motor Nozzle	Outsourced
Motor Ignition Mechanism	Commercial

Table 5.9: Commercial and In-house Components

5.8.1 Conceptual Design

The conceptual design is broken down into propulsion, aerodynamics, avionics, payload, and structural subsystems. The main component of the propulsion system is the designed solid rocket motor (SRM). The aerodynamics consist of the forebody and control surfaces, including the fins and tube, designed in Section 3.3.4. Most components of the avionics system will be commercial-off-the-shelf (COTS) products, including the purchase of the inertial measurement unit (IMU), seeker, servo/actuators, electronics, and battery. The selection of COTS components greatly increases the simplicity of this subsystem regarding design but is modeled by directly assigning a noise factor to the seeker proportional to

its cost, under volumetric and sizing restrictions to meet internal space constraints. The navigation tool development is detailed in Section 3.3.1. The payload system contains the development of the warhead as described in Section 3.3.5. The structural subsystem is responsible for the design of the semi-conventional internal supporting structure of the vehicle, the thermal protection, and the manufacturing of the control surfaces, body tube, and bulkheads.

5.8.2 Development testing

Individual Component Testing

As some of the components are designed and manufactured in-house, they have to undergo verification testing to ensure that the calculated performance matches the actual performance. The SRM will go through static firing tests to assure the quality of the motor and the accuracy of the predicted thrust curve as it fires at full thrust. The solid propellant grain of fuel and oxidant is ignited, creating a pressure difference and causing gases to exit the motor. This thrust is measured by a load cell sensor, a type of transducer that converts a given thrust to an electrical signal that can be analyzed [26]. The signal will provide a reading of how much thrust is produced and how thrust changes compared to burn time. Static fire tests can also be used to verify thermal properties and stresses on the nozzle to ensure the motor operates within structural and thermal limits [27], by extrapolating pressure cell data. An uncertainty analysis of the test rig must also be performed prior to beginning static fire testing for motor alignment and to calibrate thrust data. An example of the test stand can be seen in Figure 5.26.

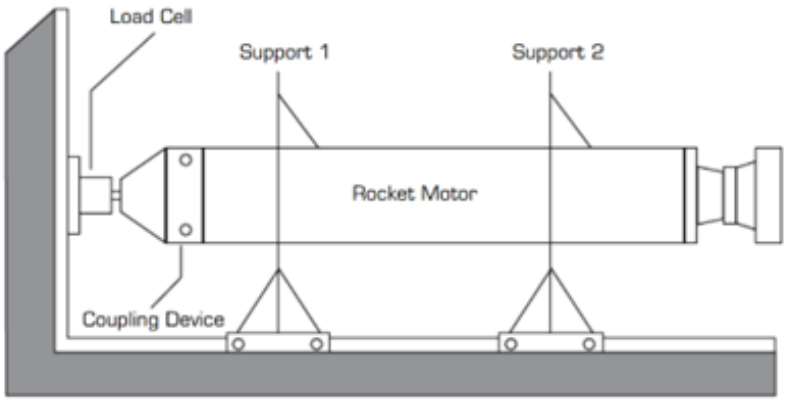

Figure 5.26: Solid rocket motor on firing test stand

Seeker testing will use infrared (IR) and laser guidance testing to determine detection range, field of view, and tracking [28]. The IR sensors can be used to carry out pattern stabilization during missile roll, drift tests, aero-thermal testing, laser heating, ramping hot dome testing, and closed-guidance loop tests. Pattern stabilization and drift tests assess tracking accuracy and alignment, and closed-guidance loop tests will provide information regarding self-correction of the missile trajectory. Aero-thermal testing evaluates seeker performance in a hostile thermal, vibration, and electrical environment to collect data aiding in the target acquisition performance assessment. The ramping hot dome test and laser heating are controlled thermal tests that simulate thermal loads on parts of the seeker and ensure that seeker performance will not be affected by extreme temperatures. Ultimately, the IR testing confirms that the seeker will uphold detection, tracking, and engagement capabilities under various stresses.

The warhead will undergo dynamic and static component level testing following US Army test and evaluation guidelines, including blast and impact lethality testing to assess structural integrity and warhead effectiveness, as well as Environmental Stress Screening (ESS), a comprehensive quality control measure that subjects the warhead to environmental stresses such as temperature cycling, vibration testing, and shock testing [29]

Component Interface Testing

Once individual components have met the necessary standards, component interface testing will be carried out to validate component system integration, as at this stage, successful interactions between in-house developed components and COTS components must be ensured. Each interacting component must undergo compatibility testing, not exclusive to designed parts compatibility, but including the interfaces between COTS parts as well, to detect any misalignment or issues with the interfacing systems. This includes vibration testing for the forebody, seeker, and warhead interface, mechanical fitting for the aerodynamic and structural body components, including the warhead, and heat management techniques for the thermal protection and electronics system. Advanced vibration test equipment will simulate high-frequency vibrations that the system would experience during flight [30]. This will also confirm that the mechanical fitting will hold under flight conditions.

The electronics system and thermal protection will be tested in a thermal cycling chamber to assess thermal decomposition of the thermal protection and damage to the electronics as they are powered on under thermal stress [31].

The missile will undergo wind tunnel testing for the airframe and control surface. For accessibility and cost reduction, a dimensional analysis technique of the Buckingham Pi theorem will be utilized to analyze the flow effects at Mach 3 in a conventional wind tunnel, as testing in supersonic wind tunnels is generally more expensive and less common [32].

Avionic software, including IMU, flight computer, GPS, and sensors, will be tested with guidance, navigation, and control (GNC) hardware-in-the-loop (HIL) simulations [33]. For the battery and avionics interface, oscilloscope-based testing will be carried out for voltage stability analysis, and systemic power testing will occur. Although more expensive, the use of COTS will decrease the cost of individual component testing as well as certification costs. The designed parts will include the cost of tooling, personnel, and testing. It is also necessary to consider the cost of interface testing.

5.8.3 System Evaluation and Validation

After development testing is complete, system evaluation and validation on missile prototypes ensues. 100 missile prototypes will be produced for the system evaluation. Ground testing of the fully integrated missile will validate reliability of the missile in compliance with DoD standards to "include formal environment, safety, and occupational health risk acceptance for test event" [34]. Static proof testing will verify load-bearing capabilities, while ground vibration tests will simulate dynamic loads and assess structural integrity. Full missile ground firing tests will validate propulsion, stability, and initial guidance function. Missile manufacturing, production, and assembly will be done at Redstone Arsenal, a DoD facility. Production will include the manufacturing of the SRM, warhead, control surfaces, and forebody. The missile ground testing will take place at Redstone Test Center (RTC), which focuses on ground testing, evaluation, and performance validation, and will have the capacity to fulfill production needs. Batch testing for production validation will use the quality management metric of Defects Per Million Units (DPMU) to account for faulty components and quality assurance. Designs will be assessed with optimality criteria to minimize deviations from optimal design performance.

The final phase of the evaluation will include demo threat testing with threat simulations as well as live fire testing to attempt to replicate realistic conditions that the interceptor will perform under, and test response to engaging threats. A sponsoring agency must be acquired, and the missile must be evaluated by the Range Safety Office for approval.

Coordination with airspace and air traffic is required by the Federal Aviation Administration (FAA) to obtain a Temporary Flight Restriction (TFR) for the missile range [35]. Demo threat testing cannot be carried out at RTC and will be moved to White Sands Missile Range via the US Army Test and Evaluation Command (ATEC), which facilitates all final system evaluation, data collection, and analysis under the Materiel Test Directorate (MT) [36].

5.8.4 Initial Operational Capability

Initial Operational Capability (IOC) will be achieved by December 2030. The COTS components, including the guidance and control electronics, communication system parts, seeker, and structural materials, will be purchased from certified manufacturers and stored in Redstone Arsenal until assembly. The SRM and warhead can also be stored at Redstone, which is a designated hazardous waste storage site and meets the Environmental Protection Agency requirements regarding explosive hazardous waste. The SRM must be separated from the warhead before being stored [37]. Carrying out all production, assembly, and testing at the same site will streamline the process from component to full production and remove the need for transportation logistics.

5.8.5 Full-Rate Production

IOC is followed by a transition to Full-Rate Production of 1000 missiles per year for 10 years as manufacturing output capabilities increase, in accordance with the production requirements from the Request for Proposal (RFP).

5.9 Concept of Operations

ARROW is designed to intercept oncoming threats within the interception range as noted by the threat scope. Moreover, the overall cost of a production unit must be kept below $ 10,000 after the effect of the learning curve is implemented. Developing a low-cost anti-missile missile can widen accessibility to defense systems, shielding military and civilian installations. The critical budget of $10,000 for this project can help streamline functional low-cost defense systems that can dramatically reduce the damage and destruction caused by aerospace warfare. This budget constraint also prioritizes the design to be simple, allowing

for rapid deployment and responsive defense. Additionally, with the low-budget design, this results in a critical advantage against foreign threats costs spent by adversaries. This can dramatically improve applicable defense for military and civilian installations.

As for ground operations, the Iron Dome will serve as the launch system for ARROW. The missile firing unit (MFU) acts as the standard land-based launcher for the Iron Dome. The MFUs allow for 20 interceptor missiles in quick-reload container canisters for quick operational defense. A full Iron Dome battery will usually field 3-4 MFUs. The capabilities of Iron Dome allow for an all-weather defense system to allow for defense near civilian and military installations on land. The Iron Dome, with the integration of ARROW will primarily serve as a counter-missile defense system.

Adversely, for naval environments, the SeaRAM launcher is used as the launch system for naval applications. The SeaRAM missile launcher replaces the Phalanx CIWS. The Phalanx CIWS acts as a turret for defense, while the RAM system contains a launcher that can carry 11 RAM missiles. Utilizing the SeaRAM RAM launcher allows for a low-cost application to provide protection over bodies of water within ARROW's range.

As for threat scope, the following assumptions are made:

- Ground ranges of 0.5 to 60 miles.
- Up to 3 g's of non-ballistic maneuvering capability.
- Speeds up to Mach 3.
- Unitary missile.
- Minimum size: 4$[in]$ in diameter, 8$[ft]$ in length, 100$[lbm]$ mass.
- Maximum size: 24$[in]$ in diameter, 20$[ft]$ in length, 4000$[lbm]$ mass.

5.9.1 Operational Environment and Weather Considerations

The Iron Dome is designed for mobility and can be rapidly deployed in various terrains and operates effectively under diverse weather conditions. The Iron Dome is specifically constructed for the Tamir missiles; however, with the size constraints of the Iron Dome MFU. The gas-generator charge within the MFU ejects a missile at a speed of roughly 20-30 m/s out of the sealed container. After clearing the launch system, the solid-fuel rocket motor ignites, accelerating the missile. As for tracking, the Iron Dome utilizes an electro-optic seeker.

Table 5.10: The dimensions and models of the missiles that are currently integrated with the Iron Dome MFU and SeaRAM.

System	Missile Model	Length	Diameter	Weight
Iron Dome	Tamir Interceptor	118.11 $[in]$	6.3 $[in]$	200 $[lbm]$
SeaRAM	RIM-116 Block 1	110 $[in]$	5 $[in]$	162 $[lbm]$
SeaRAM	RIM-116 Block 2	113 $[in]$	6.3 $[in]$	195 $[lbm]$

The SeaRAM system is applicable for deployment on multiple naval vessels. SeaRAM is designed with integration capabilities in mind, allowing for smooth integration on a variety of vessels without many modifications. The SeaRAM doesn't include a gas-ejection phase, as it directly ignites the solid fuel motor within the launching system. The initial velocity of ARROW is assumed to be zero from the launching system. The SeaRAM launcher will incorporate laser tracking to determine threat trajectories.

The missile dimensional constraints for the Iron Dome and SeaRAM launch systems have the dimensions listed in Table 5.10. These dimensions include current missile models that are used by the two different launch systems. It is assumed that ARROW will follow closely with the current integration constraints.

The Iron Dome and SeaRAM launcher systems allow for an all-weather scenario defense system. However, weather can have an induced effect on radar seeking technology. Some examples of certain impacts weather can have on radar are rain fade, radar reflection, and radar attenuation. These effects can be mitigated by using frequencies not attenuated by atmospheric weather. Another mitigation strategy for ARROW is employing space-time adaptive mapping that can differentiate threats and weather-induced radar events.

Moreover, the Iron Dome and SeaRAM launchers have manned considerations. The personnel functions and count are described in Tables 5.11 and 5.12. The Iron Dome count is an approximate count from a 100-soldier battery divided by 4 MFUs. The staff count is subject to change based on battery configuration and operational scenarios. The SeaRAM ties into the naval ship's combat system instead of relying on operators.

5.9.2 Operational Scenarios and Phases

1. **Prelaunch Phase:**

Table 5.11: Iron Dome MFUs Personnel Functions

Role	**Approximate Count per MFU**	**Primary Function**
MFU Team Leader	1	Commands the MFU crew and liaises with the Battle Management & Control (BMC) system.
Launcher (Fire Control) Operator	1	Executes launch orders, monitors missile ready status, and local fault indicators.
Vehicle Operator (Driver/Mechanic)	1	Positions the truck-towed MFU and performs basic vehicle upkeep.
Reload Technicians	8–12	Swap out spent interceptor canisters and handle on-site missile logistics.
Electronics/Maintenance Technicians	8–10	Perform diagnostics and repairs on the radar, guidance links, and launch subsystems.
Support & Security	4–8	Provide battery-level logistics, site security, and general support apportioned across MFUs.

Table 5.12: SeaRAM Missile System Personnel Functions

Role	**Approximate Count per MFU**	**Primary Function**
Dedicated On Deck Operators	0	Firing is fully automated via integrated Phalanx search and track radar and sensors.
Combat Systems Console Operator	1	Monitors and authorizes SeaRAM engagements from the Combat Information Center (CIC).
Fire Control Technician (FC)	1	Maintains launcher electronics, reloads missiles during replenishment, runs diagnostics.

- Iron Dome: The radar system onboard the Iron Dome system detects and tracks incoming threats. The threat trajectory is then used to determine the threat's possible target.
- SeaRAM: The system autonomously detects and tracks incoming threats. The integrated radar and optical sensors track the trajectory of the threat.

2. **Launch Phase:**

- Iron Dome: Upon confirmation, ARROW is launched and initiated into intercept phase.
- SeaRAM: Upon confirmation, the system launches ARROW from the 11-cell launcher and is initiated into intercept phase.

3. **Interception Phase**

   - Iron Dome: ARROW handles the tracking of the target and engages in maneuvering techniques to reach the target.
   - SeaRAM: Utilizes the dual-mode guidance system to allow ARROW to maneuver towards the target.
   - Kill Levels:
     - KK Kill:Immediate Disintegration
     - K Kill:Out of Control within 30 sec of a hit
     - A Kill:Out of Control within 5 min of a hit
     - B Kill:Out of Control within 30 min of a hit
     - C Kill:Aircraft unable to complete mission after a hit, but able to return safely to base (N/A IN THIS CASE)

4. **Post-Intercept Phase:**

   - Iron Dome: The system undergoes a reset and prepares for subsequent threats. The Iron Dome also contains the capability to handle multiple engagement scenarios.
   - SeaRAM: The system will undergo a kill assessment, during which it repositions to standby mode. Furthermore, the system remains ready to intercept additional threats as necessary.

Notional Timeline of the Engagement In the following tables 5.13 and 5.14, the notional timeline of a random engagement scenario that assembles a possible mission of the platform is presented for the Iron Dome and SeaRAM platform scenarios.

5.9.3 Operational Cost Considerations

With the use of existing launch systems, operational costs for these are covered by the operations of these systems themselves. However, an additional cost to consider is the training of the operators of these systems. However, some cost estimations for these operations can still be made. These operational cost ranges are listed and mentioned in Tables 5.15 and 5.16 for the scenario of using the Iron Dome and the SeaRAM launchers, respectively.

Table 5.13: Iron Dome Engagement Notional Timeline

Phase	Time	Description
Detection	T – 60 sec	Radar (EL/M-2084) detects incoming projectile.
Tracking and Assessment	T – 55 sec	Battle Management Control (BMC) predicts impact point and evaluates threat level.
Decision	T – 50 sec	Determines if intercept is necessary based on the threat to populated areas.
Interceptor Launch	T – 45 sec	Interceptor launched from ground launcher.
Midcourse Guidance	T – 35 sec	Uses command up-link from BMC to adjust in-flight path.
Intercept and Kill Assessment	T – 0 sec	Detonates near the target to neutralize it.
Reset and Re-Arm	T – 60 sec	Launcher reloads if needed, system returns to ready state.

5.9.4 Risk Management, Safety and Reliability

- Safety: During the pre-launch phase, the anti-missile missile can lay installed within the launch system. However, the anti-missile missile will lay within a dormant state when not tracking any threats. This "state" can be engaged from dormant to ready state within half of a second. With this then the system gives the ready status for launch. Additionally, safety arming pins must be added to the avionics and warhead subsystems so that there are no misfires prior to the engagement sequence.

- Reliability:

    1. Iron Dome: The autonomous systems within the Iron Dome allow for the minimization of human error and remain highly reliable.

    2. SeaRAM: The integrated sensor on board autonomously operates, further reducing human error and ensuring stable reliability.

As for the Risk Management, different critical scenarios are associated with possible threats to the crew and the overall operation of the systems. Thus, some mitigation strategies are proposed for some indicative scenarios in the Table 5.17.

Table 5.14: SeaRAM Engagement Notional Timeline

Phase	**Time**	**Description**
Detection	T – 30 sec	The laser tracker detects an oncoming threat.
Tracking and Assessment	T – 25 sec	Target is tracked via radar and FLIR sensors. SeaRAM's onboard control unit automatically classifies the threat based on velocity, size, and trajectory.
Decision	T – 20 sec	System verifies that threat meets engagement criteria (e.g., hostile trajectory, high closing speed). SeaRAM autonomously queues a missile launch.
Interceptor Launch	T – 18 sec	A Rolling Airframe Missile (RAM Block 1A or 2) is launched from the 11-cell SeaRAM module. Launch is vertical or near-vertical.
Midcourse Guidance	T – 10 sec	RAM missile uses passive radar homing + infrared homing for threat discrimination and flight path corrections. No external up-links are needed.
Terminal Homing	T – 0 sec	RAM missile guides toward the threat and detonates its warhead at proximity for maximum kill effect. Reaction time from detection to intercept is typically within 5–15 seconds, depending on range.
Intercept and Kill Assessment	T + 5 sec	SeaRAM uses sensors to assess interception success. If the target persists, a second missile may be auto-fired.
System Reset	T + 15 sec	System returns to ready state and reverts sensors to search mode. Launch pod automatically realigns. If needed, the crew reloads RAM missiles manually in port.

Table 5.15: Iron Dome Typical Operational Cost breakdown

Phase	**Typical Cost**
Engagement (1–2 interceptors)	$80K – $200K
Annual maintenance per battery	$500K – $1.2M
Training per year (battery crew)	$250K – $400K
Daily fuel/electrical ops	$1.5Kday – $3Kday
Interceptor resupply mission	$25K – $75K

Table 5.16: SeaRAM Typical Operational Cost breakdown

Phase	**Typical Cost**
Missile per shot	$450K – $905K
Annual maintenance per battery	$200K – $400K
Training per year (battery crew)	$5K – $10K per crew member
Daily fuel/electrical ops	negligible
Interceptor resupply mission	$50K – $200K

Table 5.17: Iron Dome Indicative Mitigation Strategies:

Risk	**Mitigation Strategy**
Saturation by swarm attacks	Layered systems, overlapping battery deployment
Wasting Interceptors	Target discrimination via trajectory analysis
Radar/weather interference	All-weather AESA radar + weather-tuned tracking algorithms
Dormant reliability loss	Routine diagnostics and shelf-life monitoring

5.10 Compliance Matrix

To demonstrate ARROW satisfies the formal requirements laid out in the RFP, a compliance matrix is outlined in Table 5.18.

Requirement	**ARROW Performance**	**Meet?**	**Analysis Location**
The missile installation shall intercept missiles up to 30,000ft in a horizontal radius of 5 miles.	ARROW intercepts threats with a design altitude of 30,000ft in a horizontal radius of 5 miles.	Yes	See Section 3.3.1, Section 3.3.2 and Section 5.4
The missile shall be compatible with safe storage and transportation for a minimum of 10 years without maintenance.	ARROW propulsion system is capable of 10-year storage.	Yes	See Section 5.9
The cost of the interceptor shall not exceed $10,000 per missile.	Mean estimated cost of ARROW is $13,563.	No	See Section 3.2 and Section 5.7
The missile shall transition from the dormant state to launch state in less than one second.	ARROW has a transition time from dormant to initial boost phase of 0.5s.	Yes	See Section 3.3.2
The missile shall intercept a target missile at speeds of up to Mach 3.	ARROW intercepts threats with design speeds between Mach0.5 and Mach3.	Yes	See Section 3.3.1, Section 3.3.2 and Section 5.4
Intercept target missile: min size 4in×8ft, 100lbm; max size 24in×20ft, 4000lbm.	ARROW intercepts threats with design geometries between 4in×8ft, 100lbm and 24in×20ft, 4000lbm.	Yes	See Section 3.3.1, Section 3.3.2 and Section 5.4
The missile shall intercept a target with a ground range between 0.5 and 60 miles.	ARROW intercepts threats for which the generated stochastic trajectories have a range of 59.5mi.	Yes	See Section 3.3.1, Section 3.3.2 and Section 5.4
The missile shall intercept a target missile with up to 3g's of maneuvering capability.	ARROW intercepts threats with stochastic maneuvers of up to 3g's.	Yes	See Section 3.3.1, Section 3.3.2 and Section 5.4

Table 5.18: Requirements verification for the ARROW surface-to-air missile design.

Bibliography

[1] R. Staff, "U.s. army awards lockheed martin $4.5 billion contract for pac-3 mse missiles," *Reuters*, Jun. 2024, Accessed April 2025. [Online]. Available: https://www.reuters.com/business/aerospace-defense/us-army-awards-lockheed-martin-45-bln-contract-2024-06-28/.

[2] C. f. S. Missile Threat and I. Studies, "Iron dome," *Missile Threat*, 2023, Accessed April 2025. [Online]. Available: https://missilethreat.csis.org/defsys/iron-dome/.

[3] W. Thomas, "Physicists argue us icbm defenses are unreliable," *FYI: Science Policy News*, Mar. 2022, Accessed: 2025-04-21. [Online]. Available: https://ww2.aip.org/fyi/2022/physicists-argue-us-icbm-defenses-are-unreliable.

[4] "Iron dome," [Online]. Available: https://www.britannica.com/topic/Iron-Dome.

[5] "2024-2025 open division missile systems deisgn competition – low-cost anti-missile missile," Jul. 2024. [Online]. Available: https://www.aiaa.org/docs/default-source/uploadedfiles/membership-and-communities/university-students/design-competitions/2024-25-mstc_missile_design_competition_2025.pdf.

[6] C. f. S. Missile Threat and I. Studies, "Rim-116 rolling airframe missile (ram)," *Missile Threat*, 2023, Accessed: 2025-04-21. [Online]. Available: https://missilethreat.csis.org/defsys/ram/.

[7] Saab, "Rbs 70 ng – new generation," *Saab*, 2021, Accessed: 2025-04-21. [Online]. Available: https://www.saab.com.

[8] G. D. Corp, "Iron dome: How it works and its capabilities," *Global Defense Corp*, 2021, Accessed: 2025-04-21. [Online]. Available: https://www.globaldefensecorp.com/2021/05/17/how-iron-dome-protects-israeli-cities/.

[9] Paul Zarchan, *Ballistic Missile Defense Guidance and Control Issues*. Science Global Security, 1998.

[10] E. L. Fleeman, *Missile design guide*. American Institute of Aeronautics and Astronautics, Inc., 2022.

[11] "Thrust curve database," [Online]. Available: https://www.thrustcurve.org/motors/search.html.

[12] E. K. Robert A. Goldbeck, "An analysis of the nike ajax missile maintenance job," American Institute of research, 1977. [Online]. Available: https://apps.dtic.mil/sti/tr/pdf/ADA034126.pdf.

[13] "Operating and support cost-estimating guide," Office of the secreatry of defense, Departement of defense, 2025. [Online]. Available: https://www.dau.edu/sites/default/files/2025-02/2025%200%26S%20Cost%20Estimating%20Guide.pdf.

[14] R. Yanushevsky, *Modern Missile Guidance*. CRC Press, 2007.

[15] C. Kopp, *Radar guided air-to-air missiles*, Accessed: 2025-05-16, 2009. [Online]. Available: https://www.ausairpower.net/TE-Radar-AAMs.html.

[16] S. Niskanen, *Openrocket technical documentation*, https://openrocket.info/documentation.html, Technical Documentation, Accessed: 2025-04-21, 2013. [Online]. Available: https://openrocket.info/documentation.html.

[17] R. C. Wilson, *Development and validation of a solid rocket motor analysis code*, Accessed: 2025-04-21, 2019.

[18] "A multi-disciplinary analysis framework for the design of small launch vehicles," ASCEND 2021, 2021.

[19] T. v. Kármán and H.-S. Tsien, "Theoretical considerations of the effects of compressibility on lifting surfaces," *Journal of the Aeronautical Sciences*, vol. 6, no. 10, pp. 379–390, 1939, Accessed: 2025-04-21. DOI: 10.2514/8.103.

[20] H. F. Nelson and D. G. Hillstrom, "Aerodynamic interference for hypersonic missiles at low angle of attack," *36th AIAA Aerospace Sciences Meeting and Exhibit*, 1998, Accessed: 2025-04-21. [Online]. Available: https://scholarsmine.mst.edu/mec_aereng_facwork/5498/.

[21] R. O'Rourke, "Navy shipboard lasers for surface, air, and missile defense: Background and issues for congress," Congressional Research Service, R41526, 2010, Accessed: 2025-04-21. [Online]. Available: https://www.everycrsreport.com/reports/R41526.html.

[22] E. T. Luan N. Dinh, *Aerothermal analysis of a space rocket during its hypersonic ascent phase*, Accessed: 2023-01-19, 2023. [Online]. Available: https://arc.aiaa.org/doi/10.2514/6.2023-0207.

[23] K. P., *Aerothermal performance constraints for hypervelocity small radius unswept leading edges and nosetips*, Accessed: 2025-04-21, 1997. [Online]. Available: https://ntrs.nasa.gov/citations/19970025227.

[24] "Airline operating costs and productivity," ICAO, February 2017. [Online]. Available: https://www.icao.int/Pages/PageNotFoundError.aspx?requestUrl=https://www.icao.int/MID/Documents/2017/Aviation%20Data.

[25] "Department of defense additive manufacturing strategy," Departement of Defense, January 2021. [Online]. Available: https://www.cto.mil/wp-content/uploads/2021/01/DoD-Additive-Manufacturing-Strategy.pdf.

[26] U. of Alabama in Huntsville, *Thesis on aerodynamics and rocket testing*, Accessed: 2025-04-22, 2021. [Online]. Available: https://louis.uah.edu/uah-theses/263/.

[27] L. Zhao and X. Zhang, "Static firing tests of solid propellant rocket motors: Uncertainty levels of thrust measurements," *ResearchGate*, 2023, Accessed: 2025-04-22. [Online]. Available: https://www.researchgate.net/publication/363490158_Static_Firing_Tests_of_Solid_Propellant_Rocket_Motors_Uncertainty_Levels_of_Thrust_Measurements.

[28] K. k. V. Scott A. Gearhart, "Infrared system test and evaluation at apl," *Johns Hopkins APL Technical Digest*, vol. 18, no. 3, pp. 290–296, 1997, Accessed: 2025-04-22. [Online]. Available: https://secwww.jhuapl.edu/techdigest/Content/techdigest/pdf/V18-N03/18-03-Gear.pdf.

[29] CBR Institute, *Missile testing and evaluation*, Accessed: 2025-04-22, 2025. [Online]. Available: https://cbrinstitute.org/missile-technology/testing-evaluation/.

[30] E. Solutions, *A comprehensive guide to vibration testing for aerospace applications*, Accessed: 2025-04-22, n.d. [Online]. Available: https://www.etssolution.com/applications/a-comprehensive-guide-to-vibration-testing-for-aerospace-applications.

[31] L. F. Wertheimer R., *Thermal decomposition analysis of rocket motors and other thermal protection systems using msc.marc-atas*, Accessed: 2025-04-22, 2003. [Online]. Available: https://tfaws.nasa.gov/TFAWS03/Data/Aerothermal%20and%20CFD%20Session/Wertheimer.pdf.

[32] L. Xu, W. Wang, and Y. Liu, "Research on optimize application of buckingham pi theorem to wind tunnel test and its aerodynamic simulation verification," *ResearchGate*, 2020, Accessed: 2025-04-22. [Online]. Available: https://www.researchgate.net/publication/342778588_Research_on_optimize_application_of_Buckingham_Pi_theorem_to_wind_tunnel_test_and_its_aerodynamic_simulation_verification.

[33] D. W. Patrick Tobbe Ph.D. Alex Matras Ph.D., *Real-time hardware-in-the-loop simulation of ares i launch vehicle*, Accessed: 2025-04-22, 2009. [Online]. Available: https://ntrs.nasa.gov/api/citations/20090034247/downloads/20090034247.pdf.

[34] Office of the Director, Operational Test and Evaluation, *Dod instruction 5000.89: Test and evaluation*, Accessed: 2025-04-22, Nov. 2020. [Online]. Available: https://www.dote.osd.mil/Portals/97/pub/policies/2020/DoDI%205000.89%20Test%20and%20Evaluation.pdf?ver=F335S087I4h7hUaH78JDLw%3D%3D.

[35] F. A. Administration, *Temporary flight restrictions (tfrs)*, Accessed: 2025-04-22, 2025. [Online]. Available: https://www.faa.gov/uas/getting_started/temporary_flight_restrictions.

[36] U.S. Army White Sands Test Center, *White sands test center*, https://home.army.mil/wsmr/unitstenants/white-sands-test-center, Accessed: 2025-04-22.

[37] National Research Council, *Storage of Separated Rocket Motors: The need for storage space for separated rocket motors*. The National Academies Press, 2010, Accessed: 2025-04-22. [Online]. Available: https://nap.nationalacademies.org/read/13439/chapter/6.